

Geochemistry, Geophysics, Geosystems

RESEARCH ARTICLE

10.1029/2019GC008287

Key Points:

- Mantle source composition has an effect on the tectonic segmentation at mid ocean ridges
- At the EPR the variations in isotopic and trace element compositions of the basalts are controlled by source composition

Supporting Information:

- Supporting Information S1
- Table S1
- Figure S1
- Figure S2
- Movie S1
- Movie S2

Correspondence to:

V. J. M. Salters,
salters@magnet.fsu.edu

Citation:

Mallick, S., Salters, V. J. M., & Langmuir, C. H. (2019). Geochemical variability along the northern East Pacific Rise: Coincident source composition and ridge segmentation. *Geochemistry, Geophysics, Geosystems*, 20, 1889–1911. <https://doi.org/10.1029/2019GC008287>

Received 4 MAR 2019

Accepted 6 MAR 2019

Accepted article online 14 MAR 2019

Published online 17 APR 2019

©2019. American Geophysical Union.
All Rights Reserved.

Geochemical Variability Along the Northern East Pacific Rise: Coincident Source Composition and Ridge Segmentation

Soumen Mallick^{1,2} , Vincent J. M. Salters¹ , and Charles H. Langmuir³ 

¹National High Magnetic Field Laboratory and Department of Earth Ocean and Atmospheric Science, Florida State University, Tallahassee, FL, USA, ²Now at Department of Earth, Environmental and Planetary Sciences, Brown University, Providence, RI, USA, ³Department of Earth and Planetary Sciences, Harvard University, Cambridge, MA, USA

Abstract New trace element abundances and isotope compositions for more than 100 mid-ocean ridge basalts from 5.5°N to 19°N on the East Pacific Rise show step function variations in isotopic composition along the ridge axis that coincide with ridge discontinuities. Transform faults, overlapping spreading centers, and devals (deviation from axial linearity) mark the separation of individual clusters of distinct isotopic composition and trace element ratios that indicate source variations. This correlated chemical clustering and morphological segmentation indicates that source composition and segmentation can be closely related even on a fine scale. Substantial chemical variations within a segment are related to source composition. This suggests that even within segments the magma transport is mainly vertical, and there is limited along-ridge transport, and there is little evidence for magma chambers that are well mixed along strike. Trace element concentrations show good correlations with isotopic compositions on a segment scale but less so on a regional scale. The trace element and isotopic variability along the northern East Pacific Rise can be explained by three mantle components: a depleted peridotite endmember, an enriched peridotite endmember, and a recycled gabbro-like component. The gabbroic component has an isotopic signature indicating an ancient origin. The high-resolution sampling indicates that within a segment the chemical variability is largely binary but that the endmembers of the binary mixing change from segment to segment. The endmembers of the binary variation within a segment are a combination of three of the endmembers.

1. Introduction

Several decades of research along the northern East Pacific Rise (EPR) have provided both regional context (e.g., Detrick et al., 1987; C. H. Langmuir et al., 1986; Macdonald, 1982) and highly detailed studies, particularly of the 9°N region (e.g., M. C. Smith et al., 2001; Wanless et al., 2010; Wanless & Shaw, 2012; Waters et al., 2011, and references therein). Despite the hundreds of publications investigating this region and abundant major and trace element data (A. Gale et al., 2014; C. H. Langmuir et al., 1986; Perfit et al., 1994), there has been no comprehensive publication of complete trace element and isotopic data despite abundant samples from the region. Here we present comprehensive trace element and isotopic data from a 1,400-km stretch of the EPR from 5.5°N to 19°N. These new data provide an essential regional context in which more detailed studies can be interpreted and permit assessment of several outstanding questions with respect to mantle heterogeneity, the significance of magma chambers, and the relationship between geochemical and petrological segmentation in this region.

There are various sizes of ridge offsets along the East Pacific Rise that exhibit a hierarchical structure between large offset transforms and small offsets of the axial fissure swarm (Langmuir et al., 1986). A convenient nomenclature for these ridge offsets that applies to fast spreading ridges was provided by Macdonald et al. (1988, 1991) and White et al. (2002). First-order discontinuities are transform faults that are stable and long-lived features (Schouten & Klitgord, 1982) and can persist for tens of millions of years (Carbotte et al., 2015). Second-order discontinuities are overlapping spreading centers (OSCs), with separation of 3–20 km that produces a clear offset of the axial high and a basin between the overlapping ridges. These discontinuities can persist for millions of years and migrate along ridge axis (Carbotte et al., 2015). Third- and fourth-order discontinuities are the deviations in axial linearity (devals of Langmuir et al., 1986) or small OSCs and are considered to be more transient features that migrate along the ridge. Migration and evolution of the

second- to fourth-order discontinuities have been related to changes in the direction of the plate motion (Carbotte & Macdonald, 1992; Hey et al., 1988; Hey & Wilson, 1982; Pockalny et al., 1997) or variations in delivery of melt to the crust (Langmuir, 1987; Langmuir et al., 1986; Macdonald et al., 1988; Macdonald et al., 1991) that have now been imaged seismically as discrete nodes of mantle melt delivery at the base of the lithosphere (Toomey et al., 2007). Our study area includes a range of offsets from first order to fourth order (Carbotte et al., 2013; Langmuir et al., 1986). Previous studies have shown that individual ridge segments down to the scale of devals have isolated magmatic systems (Langmuir et al., 1986; Perfit et al., 1994; Reynolds et al., 1992; Smith et al., 2001). Recent studies have shown that third- and higher-order discontinuities at the EPR coincide with disruptions in the magma lens underneath the ridge, and these discontinuities also represent magmatic separations (Carbotte et al., 2015; Langmuir et al., 1986). The current study aims to determine the scale of heterogeneities in the mantle and the possible connection between source characteristics and the physical expressions of the ridge. Key issues that can be addressed with the new data include the following: (1) Is magma ascent focused at segment centers from where they flow to segment ends in crustal plumbing systems, or Do they rise at multiple points along the ridge axis? (2) Is there melt transport across discontinuities? (3) What is the length scale of chemical continuity and can it effect segmentation? Other fundamental questions that can be addressed with this data set are the importance of magma chamber processes for trace element variations and presence and identification of source variations.

2. Geological Setting

The 1,400-km-long ridge section from 5.5° to 19°N EPR is a fast-spreading ridge section (90–110 mm/year, full spreading rate), with small variations in spreading rate that increase from north to south. The ridge is far removed from any known hot spot, and ridge depths are between 2,300 and 3,000 m except south of the Orozco Fracture Zone where it deepens from 2,800 to 3,500 m over 30 km (Carbotte et al., 2004; Macdonald, 1982). The shallowest ridge segment is north of Orozco, which also shows sharply lower mantle Bouguer anomaly indicating thicker crust (Carbotte et al., 2015). There are several small seamounts on either side of the ridge on the Cocos Plate (east) and the Pacific Plate (west; see Figure 1). In addition, off-axis near-ridge extrusions have been identified (Perfit et al., 1994; Reynolds & Langmuir, 2000; Smith et al., 2001; Turner et al., 2011; Waters et al., 2013; Zou et al., 2002) between 9°N and 11°N. With exception of the segment north of Orozco, the limited depth variation and the small number of seamounts argue for a relatively uniform melt production along this part of the ridge system.

Along-axis seismic surveys reveal an axial magma chamber (AMC) reflector underlying part of the ridge (Carbotte et al., 1998; Detrick et al., 1987; J. M. Sinton & Detrick, 1992). In some places magma chambers are found to be present beneath the ridge for up to 100 km (9.11–10.21°N), albeit with important changes in depth that suggests that there may not be continuity (Carbotte et al., 2015). These studies also observed that the magma chambers become narrower and sometimes disappear near transform faults. Seismic evidence for off-axis melt bodies has also recently been found between 9.5°N and 10.0°N (Canales et al., 2012; Durant & Toomey, 2009; Han et al., 2014).

The ridge between the Siqueiros Fracture Zone and 19°N is segmented by 4 large transform faults, 3 OSCs, 1 nontransform offset, and 25 devals (Carbotte et al., 2015). Between the Siqueiros Fracture Zone and 5.5°N data are much scarcer but at least one OSC is observed at 7.21°N. The transform faults are all associated with a change in ridge depth across the transform. Figure 1 shows the sample coverage as well the ridge discontinuities that are recognized in this study through chemical differences.

3. Previous Work

Samples discussed in this study are from within 500 m of the ridge axis, which minimizes the chance that they represent off-axis eruptions. The existing major element and trace element chemistry of basalts along the northern EPR, 5.5–14.5°N (Goss et al., 2010; Langmuir et al., 1986; Perfit et al., 1994; Reynolds et al., 1992; Smith et al., 2001; Wanless et al., 2010; Wanless & Shaw, 2012; Waters et al., 2011), reveal chemical domains that are bounded by discontinuities, including OSCs and devals (Langmuir et al., 1986). Large ridge offsets are expected to influence the nearby erupted basalt as it places relatively cold and thick lithosphere next to the ridge crest, potentially reducing mantle melting and potentially increasing crystal fractionation

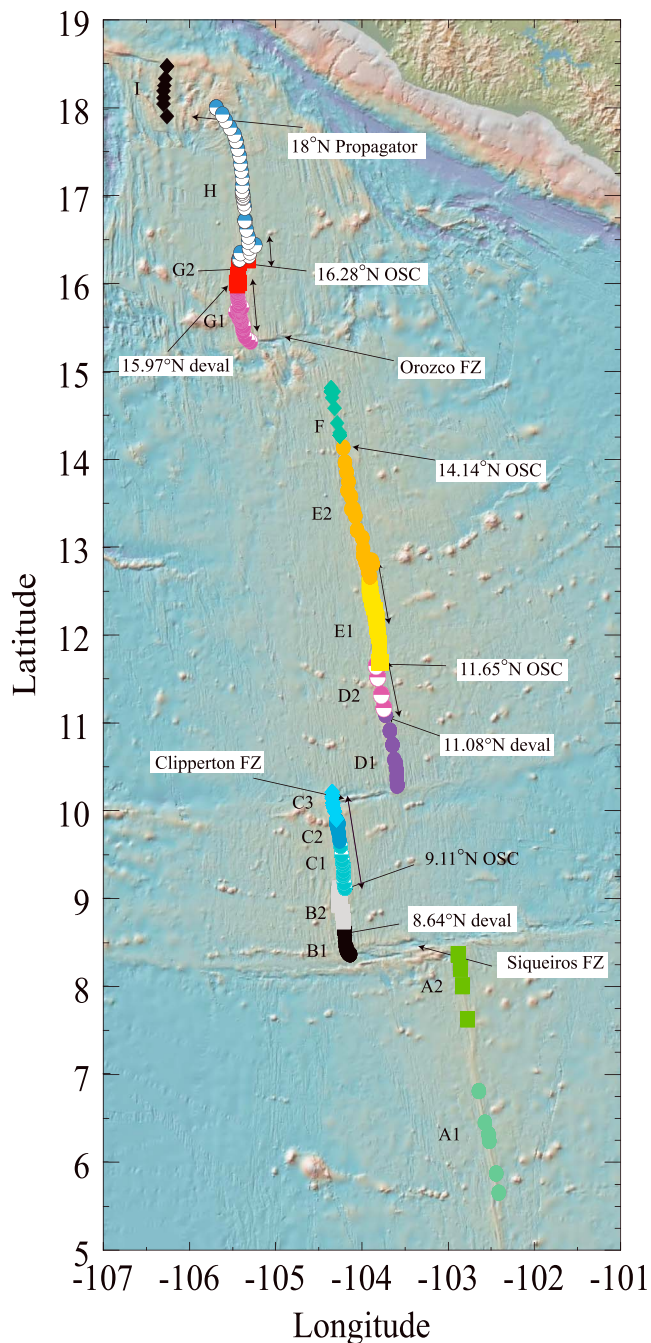


Figure 1. Sample locations for new analyses presented in this manuscript. Also indicated are the ridge discontinuities that are related changes in chemistry, with change in sample location symbols across those boundaries. FZ = Fracture Zone; OSC = Overlapping Spreading Center. Arrows parallel to the ridge axis indicates locations where an axial magma chamber reflector has been imaged seismically.

resulting in many locations in chemically more diverse basalts at the segment end compared to its center (Bender et al., 1984; Christie & Sinton, 1981; Langmuir & Bender, 1984; Perfit & Fornari, 1983). OSC's and propagating rifts have also been found to separate different magmatic domains (e.g., (Christie & Sinton, 1981; Klein, et al., 1988; Langmuir et al., 1986; Schilling et al., 1983). More intriguing are the chemical offsets at devals. While seismic studies show that these features are likely controlled by the spatial distribution of melt supply from the mantle (Toomey et al., 2007), at the surface their expression is an offset in the axial fissure swarm and thus may separate eruption units. Such small offsets would not be expected a priori to correlate with mantle source boundaries. This study presents a comprehensive published isotopic study that can address the question of small ridge offsets and how they may or may not be related to the mantle beneath the ridge.

Available major and trace element and isotope data for 5.5°N to 19°N EPR are from Castillo et al. (2000), Donnelly (2002), Gale et al. (2013), Reynolds et al. (1992), Sims et al. (2002), and Su (2002) and PetDB. Isotope studies are mostly limited to the ridge north of 11.75°N (Castillo et al., 2000; Donnelly, 2002) and near 9.50°N (Goss et al., 2010; Mougél et al., 2014; Sims et al., 2002; Sims et al., 2003; Waters et al., 2011).

The major elements show a wide range of variation: $\text{SiO}_2 = 48.50\text{--}67.54$ wt.%, $\text{MgO} = 0.95\text{--}10.80$ wt.%, $\text{Al}_2\text{O}_3 = 12.21\text{--}16.82$ wt.%, $\text{Na}_2\text{O} = 2.00\text{--}4.72$ wt.%, and $\text{TiO}_2 = 0.84\text{--}3.32$ wt.%. The samples selected for this study are basaltic in composition ($\text{SiO}_2 \leq 52$ wt.%) except for three basaltic andesites ($\text{SiO}_2 = 52.23\text{--}56.60$ wt.%) and one andesite ($\text{SiO}_2 = 61.10$ wt.%). The major element compositions range from almost unfractionated to highly fractionated compositions ($\text{Mg}\# = 0.20\text{--}0.68$). None of the samples has $\text{Mg}\#$ high enough to be primary melt compositions ($\text{Mg}\# > 0.72$). The following sections discuss only the samples with $\text{Mg}\# > 0.45$.

$\text{K}_2\text{O}/\text{TiO}_2$ is widely used as an indicator of degree of enrichment (Perfit et al., 1994; J. R. Reynolds et al., 1992; J. M. Sinton et al., 1991). Gale et al. (2013) proposed a reclassification of MORB, where N-MORB refers to the most common ridge composition sampled more than 500 km from a hot spot and D-MORB is the group of most depleted compositions. N-MORB by this definition has an average $\text{K}_2\text{O}/\text{TiO}_2$ of 0.09, D-MORB has an average $\text{K}_2\text{O}/\text{TiO}_2$ of 0.06, and E-MORB $\text{K}_2\text{O}/\text{TiO}_2$ averages 0.26. The $\text{K}_2\text{O}/\text{TiO}_2$ for the N-EPR ranges from 0.01 to 0.33, from D-MORB to E-MORB. The mean $\text{K}_2\text{O}/\text{TiO}_2$ excluding the few andesites is 0.099, similar to the N-MORB global average. Langmuir et al. (1986) found that Ba/TiO_2 and Sr contents as well as major elements display chemical shifts across discontinuities, even at the level of devals. This observation led them to conclude that crust generation along the EPR is dominated by multiple vertical melt channels feeding the crust, and they found limited evidence for a central supply at the segment center and shallow level flow toward the segment ends.

There have been a number of studies, some in great detail, that document the major and trace element variations in young oceanic crust at the EPR between 9°N and 10°N (Goss et al., 2010; Perfit et al., 2012; Smith et al., 2001; Wanless et al., 2012; Wanless & Shaw, 2012). These studies have argued that a large part of the compositional variation is related to fractional crystallization and mixing of more evolved melts with parental ones. This is especially apparent at the OSCs at 9°N (Wanless et al., 2012) and at 9.62° (M. C. Smith et al., 2001). Near the OSC more evolved magmas, compositions up to dacite,

can erupt. In addition, the abundance of E-MORB increases near the OSC. Away from the OSC E-MORB is virtually absent on-axis. Basalts from the EPR between 9°N and 10°N show ample evidence for fractional crystallization and mixing at shallow levels. Melt inclusions at three locations show that the majority of the inclusions last equilibrated at depths of less than 2.5 km, which coincides with the depth of the AMC (Wanless & Shaw, 2012).

Castillo et al. (2000) proposed that the chemical and isotopic variability between 11.65°N and 15.00°N EPR can be explained by the three mantle components: a depleted mantle component, a seamount-type enriched component, and an Indian MORB-type mantle component. Based on samples with somewhat higher $^{207}\text{Pb}/^{204}\text{Pb}$ for a given $^{206}\text{Pb}/^{204}\text{Pb}$, they further concluded that the Indian mantle component becomes prevalent north of the 14.14°OSC.

Donnelly (2002) studied the northern region and likewise proposed a three-component mantle to explain the combined trace element and isotope ratios north of the Orozco Transform Fault from 15.37°N to 16.28°N. However, instead of an Indian MORB-type mantle component, a recycled gabbroic component (based on high Ba, Sr content and low $^{206}\text{Pb}/^{204}\text{Pb}$ - $^{208}\text{Pb}/^{204}\text{Pb}$ and moderate $^{207}\text{Pb}/^{204}\text{Pb}$) in addition to a depleted component and an enriched component is proposed to cause the geochemical variability. A comprehensive trace element and isotope study by Waters et al. (2011) of two ridge sections around 9.8°N, several kilometers in length, also argued for three components, where most of the variation is the result of two-component mixing and the third component plays a minor role. Mougel et al. (2014) found that north of the Orozco fracture zone the basalt composition changes drastically with a drop in Mg#, high La/Sm, low Zr/Nb, and unradiogenic Pb and Nd isotopes combined with radiogenic Sr isotopes. They also argue for the presence of ancient recycled gabbro in the basalts just north of the Orozco Fracture zone (Mougel et al., 2014).

4. Analytical Techniques

For trace elements analyzed at FSU, approximately 5 mg of handpicked glass was dissolved in an HF:HNO₃ (3:1) mixture. Trace element concentrations were determined by ICP-MS (ThermoFisher ELEMENT2) on a 2% HNO₃ solution with 100-ppm total dissolved solid. The concentrations were calculated using the values for BHVO-1 (Eggins et al., 1997) as a standard. Signal drift during an analytical session was corrected for by using indium as a monitor. Samples and standards were spiked with 1 ppb In. To minimize drift corrections, samples were measured in a short sequence of one blank, one standard BHVO-1, three samples, and one standard (BIR-1 or BCR-1). Concentrations were calculated using linear interpolation between the two BHVO-1 after normalizing intensities to Indium. Rock standards (BIR-1, $n = 9$ and BCR-1, $n = 18$) were measured to determine external reproducibility and accuracy. For most of the elements reproducibility was within 5% and the calculated concentrations agree very well with the reported value.

Trace elements at Harvard were measured by solution nebulized-inductively coupled mass spectrometry. Fifty milligrams of handpicked rock or glass chips was digested in an HF:HNO₃ mixture. The sample was diluted 1:5000 using a matrix solution of 0.2N HNO₃ with Ge (10 ppb), In (3 ppb), Tm (3 ppb), and Bi (3 ppb) as internal standards for drift correction. Runs were made in both normal and CCT mode in order to obtain both major and trace elements. Measurements were obtained on a Thermo X series quadrupole. Standard powders BHVO-2, DNC-1, JB-2, and W-2 as well as two in-house standards (powdered MAR and handpicked glass chips of VE-32) were used to generate calibration curves.

Comparison of the FSU and Harvard generated data shows very good agreement in element-element plots of elements that show similar behavior like Ho-Y, Sm-Zr, Sm-Eu, U-Th, and Nb-Th. On these plots the data from the two laboratories are indistinguishable from each other. Although the difference is small, Gd is systematically higher in the Harvard data compared to the FSU data. The REE pattern of the Harvard data shows an average of 8% excess of Gd compared to its neighboring REE, while FSU data show an average of 3% deficit of Gd compared to its neighboring REE. These differences, however, do not effect our interpretation of the data.

The isotopic compositions were analyzed on approximately 100 mg of fresh glass, which was handpicked under binocular microscope and cold leached with 2.5N HCl for about 15–20 min. The leached fraction was rinsed several times using 18MΩ deionized water and then quartz distilled water and finally dissolved in HF:HNO₃ (3:1) mixture using standard technique. Pb, Hf, Sr, and Nd were separated from

the same aliquot following the techniques outlined in Stracke, Zindler, et al. (2003). Sr isotope ratios were measured by thermal ionization mass spectrometer in dynamic mode on a Finnigan MAT 262 RPQ mass spectrometer. $^{87}\text{Sr}/^{86}\text{Sr}$ ratios are corrected for fractionation to $^{86}\text{Sr}/^{88}\text{Sr} = 0.1194$. Long-term average of Sr standard E & A yields a value of 0.708004 ± 18 ppm ($n = 25$, 2σ). $^{87}\text{Sr}/^{86}\text{Sr}$ of the samples are reported relative to the accepted ratio of E & A standard ($^{87}\text{Sr}/^{86}\text{Sr} = 0.70800$). Nd-Pb-Hf isotope ratios were measured on a ThermoFinnigan NEPTUNE MC-ICP-MS. $^{143}\text{Nd}/^{144}\text{Nd}$ ratios are corrected for fractionation to $^{146}\text{Nd}/^{144}\text{Nd} = 0.7219$. $^{176}\text{Hf}/^{177}\text{Hf}$ ratios are corrected for fractionation to $^{179}\text{Hf}/^{177}\text{Hf} = 0.7325$. Repeated measurements of Nd standard La Jolla and Hf standard JMC-475 yielded an average value of $^{143}\text{Nd}/^{144}\text{Nd} = 0.511839 \pm 36$ ppm ($n = 110$, 2σ) and $^{176}\text{Hf}/^{177}\text{Hf} = 0.282147 \pm 47$ ppm ($n = 108$, 2σ). $^{143}\text{Nd}/^{144}\text{Nd}$ and $^{176}\text{Hf}/^{177}\text{Hf}$ ratios of the samples are reported relative to the accepted ratio of the standard— $^{143}\text{Nd}/^{144}\text{Nd} = 0.511850$ (La Jolla) and $^{176}\text{Hf}/^{177}\text{Hf} = 0.282160$ (JMC 475).

Pb isotope ratios were measured using a Tl spike to correct for mass fractionation with ratios corrected to $^{203}\text{Tl}/^{205}\text{Tl} = 0.4188$. Samples and standard were spiked with Tl to obtain a Pb/Tl ratio of approximately 6. Long-term averages of the Pb standard NBS-981 are $^{206}\text{Pb}/^{204}\text{Pb} = 16.9294 \pm 136$ ppm, $^{207}\text{Pb}/^{204}\text{Pb} = 15.4824 \pm 164$ ppm, and $^{208}\text{Pb}/^{204}\text{Pb} = 36.6698 \pm 211$ ppm ($n = 100$, 2σ). Pb isotope ratios are reported relative to the accepted values of NBS 981 ($^{206}\text{Pb}/^{204}\text{Pb} = 16.9356$, $^{207}\text{Pb}/^{204}\text{Pb} = 15.4891$, and $^{208}\text{Pb}/^{204}\text{Pb} = 36.7006$; Todt et al., 1996).

5. Results

The samples for which we report additional data were collected during CHEPR (Langmuir et al., 1986), VENTURE (Reynolds, 1995; Reynolds & Langmuir, 2000), and PANAROMA (Donnelly, 2002; Langmuir et al., 1988) expeditions. The new trace element abundances and isotopic compositions of basalts are presented in Table S1 in the supporting information and significantly increases the amount of trace element and isotope data for the N-EPR. The data we discuss here and which we present in the figures also include data from Castillo et al. (2000), Donnelly (2002), Goss et al. (2010), Langmuir (2013), Langmuir et al. (1986), Mougél et al. (2014), Su (2002), and Wanless et al. (2012). We have not included the data of Sims et al. (2003, 2002) as some of these data plot consistently as outliers.

The samples range in $\text{K}_2\text{O}/\text{TiO}_2$ from 0.03 to 0.32, representing 90% of the $\text{K}_2\text{O}/\text{TiO}_2$ variation of MORB (see Figure 2). Based on the $\text{K}_2\text{O}/\text{TiO}_2$ ratios 32% of the samples are D-MORB with less than 0.08 $\text{K}_2\text{O}/\text{TiO}_2$ and have $(\text{La}/\text{Sm})_{\text{N}}$ of 0.57 ± 0.1 , consistent with the global average D-MORB for $(\text{La}/\text{Sm})_{\text{N}}$ of 0.60. Fifty percent is N-MORB with $\text{K}_2\text{O}/\text{TiO}_2$ between 0.08 and 0.13 and have average $(\text{La}/\text{Sm})_{\text{N}}$ of 0.68 ± 0.12 , consistent with global N-MORB with $(\text{La}/\text{Sm})_{\text{N}}$ of 0.73 (Gale et al., 2013). At $\text{K}_2\text{O}/\text{TiO}_2 > 0.12$, the $(\text{Ce}/\text{Yb})_{\text{N}}$ ratio transitions from <1.0 to >1 , while $(\text{La}/\text{Sm})_{\text{N}}$ remains <1 , consistent with the slightly “humped” pattern that is characteristic of many MORB (Hofmann, 1988). Samples with $(\text{La}/\text{Sm})_{\text{N}}$ greater than 0.9 and $\text{K}_2\text{O}/\text{TiO}_2$ greater than 0.15 are transitional to enriched and make up 18% of the samples. Only 4% of samples have $(\text{La}/\text{Sm})_{\text{N}}$ greater than 1. Note that all transitional to enriched samples have $\text{Mg}\# \leq 0.50$.

Our new data show that most of the N-EPR has relatively limited variation in Sr and Nd isotopic composition (Figure 3a) but large variations in Pb isotopes with $^{206}\text{Pb}/^{204}\text{Pb}$ ranging from 17.45 to 18.61 (Figure 3b). About 50% of the Pb isotope variation is from the segment just north of the Orozco Transform. Excluding the segment north of the Orozco Transform, 80% of the Nd and Sr isotopic compositions lie between 0.5131 and 0.5132 and 0.7024 and 0.7029, respectively. Incompatible element ratios that are not easily changed by melting or crystal fractionation also show significant variation with Ba/Th varying by a factor of 8, La/Nb and Zr/Nb by a factor of 6, La/Sm by a factor of 5, and La/Th and La/Nb by a factor of 4. Previous studies on the northern EPR of smaller geographic extent found that two source components could explain the observed geochemical variations; see, for example, Sims et al. (2002), although the Pb isotopic variation hints the presence of a third component (Waters et al., 2011). Over the extended geographic range of this study two source components, even as each component is allowed to have a range in composition, it cannot explain the complete data.

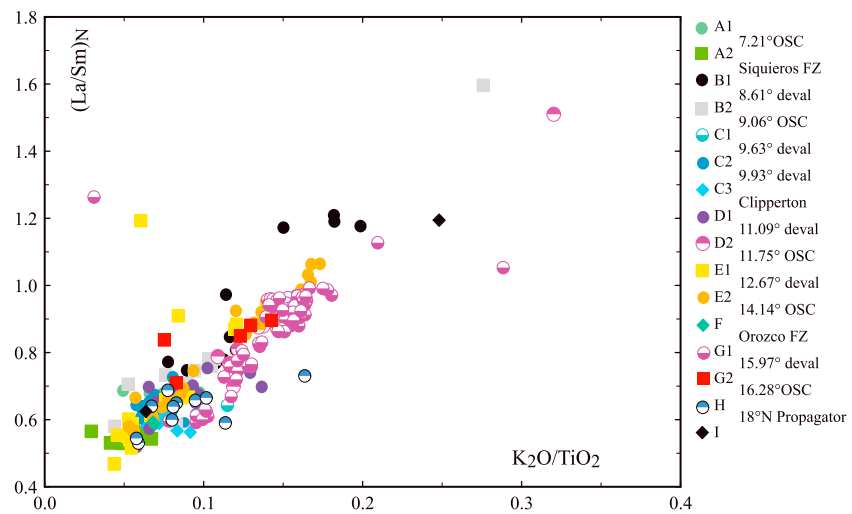


Figure 2. K_2O/TiO_2 versus chondrite normalized La/Sm for segment A through I along the EPR. Normalization from McDonough and Sun (1995). Except for segments F, H, and I, segments can be further subdivided based on third-order discontinuities. The symbol code used in this figure will also be used in the subsequent figures. The EPR data used in this and all subsequent figures are from Table S1 and the following references: (Castillo et al., 2000; Donnelly, 2002; Goss et al., 2010; C. E. Langmuir, 2013; Mougél et al., 2014; Sims et al., 2002; Su, 2002).

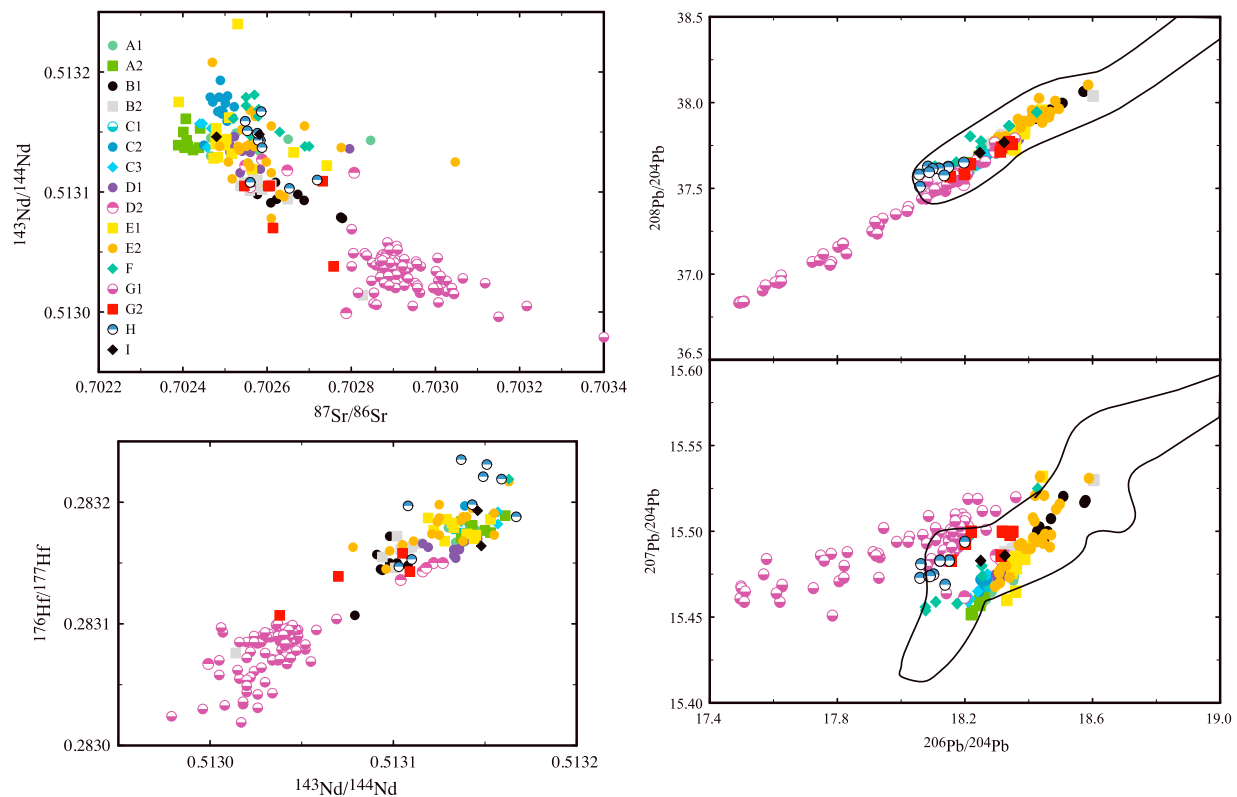


Figure 3. Sr, Nd, Hf, and Pb isotope variations of the East Pacific Rise. Individual segments identified by composition have different symbols. Slopes of variations of individual segments are different in $^{206}Pb/^{204}Pb$ - $^{207}Pb/^{204}Pb$ space, requiring a minimum of three endmembers to explain the Pb isotope data. Field for EPR seamounts is also indicated (Niu et al., 2002; Niu & Batiza, 1997; Zhang et al., 2016).

6. Discussion

6.1. Magma Chamber Effects

It is commonly believed that at fast spreading rates melts undergo mixing in AMCs (Rubin et al., 2009; Rubin & Sinton, 2007). AMCs occur more often beneath fast and intermediate spreading ridges (Carbotte et al., 1998; Detrick et al., 1987; Sinton & Detrick, 1992) and are rarer beneath the slow spreading ridges (Detrick et al., 1990; Singh et al., 2006). At the EPR it has often been proposed that apparent chemical homogeneity of the ridge basalts is caused by efficient mixing and buffering by an AMC beneath the ridge (Batiza et al., 1996; Perfit et al., 1994; Perfit et al., 2012; Sims et al., 2002; Sims et al., 2003). Rubin and Sinton (2007) and Rubin et al. (2009) argued that at fast-spreading ridges, where the magma supply is high, AMCs produce a higher degree of crystal fractionation and more extensive mixing of magmas. Consequently, the basalts processed through such a magma chamber should be more homogeneous as differences in input magmas are averaged out and have lower Mg#. Bergmanis et al (2007), however, found substantial variations in magma composition of historical lavas along a small portion of the southern EPR where a continuous AMC reflector exists, suggesting that the magma chambers on time scales of centuries have limited ability to produce homogeneous magmas.

In the 5–19°N area ridge segment C has an AMC reflector along almost its entire length, while segments D, E, and G are partly underlain by an AMC (Carbotte et al., 1998; Detrick et al., 1987; Sinton & Detrick, 1992). It should be noted, however, that the AMC is not at a constant depth and thus not necessarily continuous (Carbotte et al., 2013; Carbotte et al., 2015). The combination of the isotopic composition and trace element variations over a large section of the ridge system that has robust magmatism allows us to assess the importance of magma chamber processes (O'Neill & Jenner, 2012) and to what extent they homogenize erupted magmas on a segment scale.

If magma chamber processes dominate trace element contents and ratios of MORB, it would permit the argument that progressive mixing in steady state magma chambers will lead to large trace element enrichments (O'Hara, 1977). Coogan and O'Hara (2015), Jenner et al. (1981), and O'Hara (1977) have suggested that these enrichments can mimic those of mantle melting. It is important to recognize, however, that for magma chambers undergoing fractional or equilibrium crystallization these large enrichments occur only when there are very large mixing increments between relatively primitive and highly evolved magmas (e.g., the entering magma increment occupies half the magma chamber volume). Otherwise, for small mixing increments, enrichments are restricted to the equilibrium liquid line of descent (Langmuir & Hanson, 1980). Lissenberg et al. (2013) shows pervasive reactive melt migration affecting the lower oceanic crust at the Hess Deep, but it is as of yet unclear to what extent this affects the erupted melts. It should be pointed out that in the study area discussed here the complete trace element variation can be found at the high MgO end of the compositional spectrum and the trace element variations correlate with the isotopic composition. This strongly suggests that the trace element variations are not related to shallow level crustal processes. While magma chamber processes lead to limited mixing and influence the extent of differentiation, (e.g., Rubin & Sinton, 2007), their effects on trace element ratios derived from a homogeneous parental magma are not supported by the inclusions of isotopic data.

The same conclusion is evidenced from consideration of the trace element data alone. There is a general misconception in the literature that periodically replenished magma chambers can replicate the effects of melting (e.g., the references above). This is not the case, because the mineralogy of crustal processes is distinct from melting mantle lherzolite. All MORB with <8 wt.% MgO have plagioclase on the liquid line of descent, and all gabbroic rocks have plagioclase as a dominant phase. During crystallization, plagioclase makes up some 50% of the crystallizing assemblage. Plagioclase has a partition coefficient for Sr of about 2, leading to a bulk distribution coefficient of 1. This contrasts markedly with the mantle partition coefficient for Sr of about 0.02. Plagioclase also takes up Ba, and the partition coefficient for Ba (~0.3) is higher than that for La (~0.1) and much higher than Rb (~0.02). During crustal processes, therefore, Ba is more compatible than La and Rb, while during mantle processes Ba is more incompatible than La and about the same as Rb. Crustal processes involving plagioclase keep Sr essentially constant, as Ba/La declines, and other incompatible elements that are not included in plagioclase increase. This leads to clear tests for the importance of magma chamber processes in controlling the trace element variations. As rare earth elements increase, there should be a larger Sr (and Eu) anomaly, and as Ba increases, the Ba/La

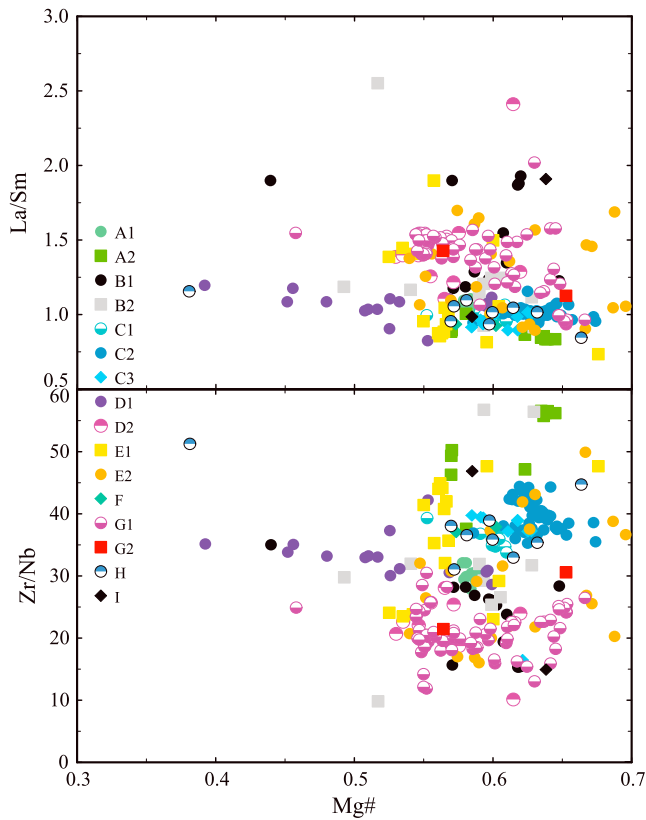


Figure 4. La/Sm and Zr/Nb versus Mg# as examples that most of the variation in trace element ratios is present in the relatively unfractionated basalts.

ratio should decrease. There should be no correlation between Sr contents and enrichment in incompatible elements.

If there are large mixing increments between a high MgO magma and highly differentiated magmas, then the concave upward shape of the liquid lines of descent permits different samples that mix with a variety of highly differentiated magmas to have large variations in incompatible elements at the same MgO content (see also Perfit et al., 2012). So the large incompatible element variations at high MgO (see Figure 4) in this region are not necessarily evidence against the magma chamber hypothesis. But the tests outlined above do provide definitive tests. Figure 5a shows a correlation between La/Sm ratios and Sr concentrations. Large variations in La/Sm at constant Sr content are expected if periodically replenished magma chambers as envisaged by O'Neill and Jenner (2012) and Coogan and O'Hara (2015) exist. Furthermore, as La or Ba contents increase, a replenished magma chamber should cause the Ba/La ratio to decrease, but data show that Ba/La ratio increases (see Figure 5b). Ba sees the same high degree of enrichment than Th (see Figure 5c), while less enrichment is expected if crustal processes are important, because Th remains highly incompatible during crustal processes while Ba does not. All of these lines of evidence are consistent with mantle control on the trace element variations, and periodically replenished magma chambers are effectively ruled out as an important control on the trace element observations, on the East Pacific Rise, and elsewhere.

6.2. Geochemical Variations as a Function of Latitude

Gradients in isotopic composition in the Atlantic and Indian Oceans are often influenced by hot spots (e.g., (Meyzen et al., 2007; Schilling, 1975) which impose gradients over several hundred kilometers in isotopic and trace element composition. The northern EPR investigated here does not have any identified hot spots and yet exhibits substantial isotopic heterogeneity. Meyzen et al. (2007) suggest that because the Pacific basin is not influenced by continental lithosphere, it reflects more distributed mantle upwelling, which is also consistent with mantle tomographic images suggesting broad and deep upwelling associated with the East Pacific Rise (e.g., (Méglin & Romanowicz, 2000). Shear velocities beneath the northern East Pacific Rise are also associated with slow velocities to depths of 300 km. This region thus appears to reflect a general upwelling of the upper mantle, and isotopic variations would be expected to reflect the components of upper mantle composition in this region rather than the particular flavor of hot spot. The isotopic data then provide constraints on this composition and the components that make it up and also on how magmatic segmentation may or may not be related to relatively short-scale variations in mantle properties.

For the northern EPR it has been shown that magmatic diversity in terms of major and trace elements varies from one ridge segment to another and occurs on the scale of first- to fourth-order ridge discontinuities (Langmuir et al., 1986; Reynolds, 1995), with “magmatic segmentation” referring to distinct chemical characteristics from one segment to another. The isotopic data presented here allow assessment whether the magmatic segmentation can be extended to source compositions.

There are significant and systematic isotopic variations with latitude along the ridge. Figure 1 shows the division of the ridge in segments and subsegments that are recognized as tectonic segments as well as “isotopic” segments. The isotopic segmentation is recognized as basalts from a segment differing in isotopic composition from basalts from neighboring segments. Segments, separated by either fracture zone or significant OSC, are labeled alphabetically from south to north. Subsegments that are separated by third- or fourth-order discontinuities and are also recognized by a change in isotopic composition of the basalts are numbered increasing northward. The along-axis variation in isotopic composition and incompatible trace element ratios is also shown in the supporting information (Figures S1 and S2). However, the difference between segments is best shown when two or three chemical parameters are shown and

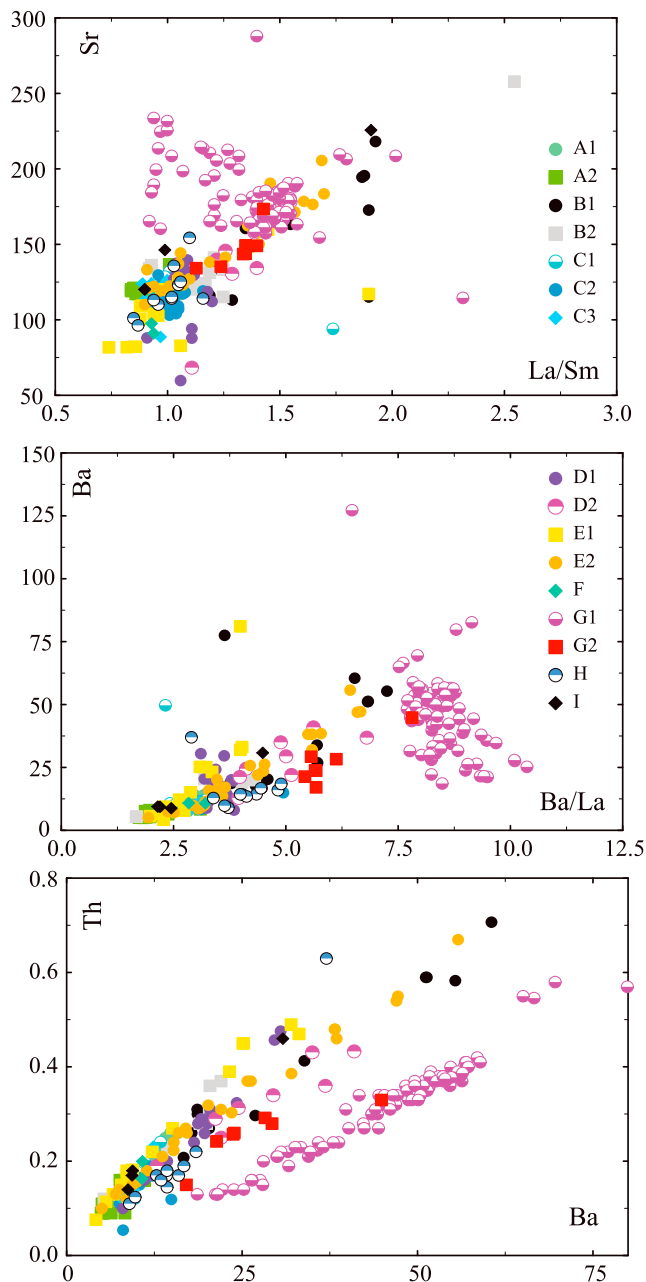


Figure 5. Trace element variation testing the importance of low-pressure fractionation. A. La/Sm versus Sr content showing an increase in Sr with La/Sm. This increase cannot be explained by shallow magma chamber processes and has to be related to source effects. B. Ba versus Ba/La. Samples in B and C are only from south of the Orozco Fracture zone as the segment north of it shows unusual Ba enrichments. Low-pressure fractionation would increase Ba/La with increasing Ba concentration. This is not observed. C. Ba versus Th. If the enrichment is due to plagioclase fractionation, Th should enrich more than Ba. OSC = overlapping spreading center.

samples are grouped by segment. These are shown in graphs such as Figure 6 or supporting information movies. It is the combination of several parameters that shows the differences between adjacent segments as detailed below.

The southernmost ridge segment of our study area (segment A) is between the 5.5°N OSC and the Siqueiros Fracture Zone and can be further divided by a small offset OSC at 7.21°N. All analyzed basalts from this segment are D- or N-MORBs, and those in the northern part (A2) are the most depleted in terms of trace elements and have among the lowest K_2O/TiO_2 ratios of our study area. Although there is a gap in the isotope data between 6.80°N and 8.00°N, the basalts north of the 7.21°OSC have lower $^{206}Pb/^{204}Pb$ and $^{87}Sr/^{86}Sr$ and more radiogenic $^{143}Nd/^{144}Nd$, and there is almost no overlap in Pb isotopic compositions (see Figure 6a). The clustering of compositions north and south of the 7.21°OSC is observed for all four isotope systems as well as in trace element ratios like La/Th, La/Nb, and Ba/Th.

There is a significant change in isotopic composition across the Siqueiros FZ, and in any plot of two isotopic compositions the fields for the basalts from the segment north of the Siqueiros FZ (segment B) and those directly south form separate clusters (see Figure 6a). This difference in composition again occurs for all isotope systems. In addition, the isotopic compositions of the basalts from segment B, between the Siqueiros FZ and the 9.11°N OSC, form two clusters separated by a deval at 8.61°N. The difference in composition of the clusters separated by the 8.61°N deval is especially clear for the Pb isotope systems where there is no overlap in composition including $^{208}Pb/^{206}Pb$. Except for one E-MORB, the N-MORBs north of 8.61°N have less radiogenic $^{206}Pb/^{204}Pb$ and $^{208}Pb/^{204}Pb$ than those to the south (see Figures 3b, 3c, 6a, and S1). Carbotte et al. (2015) indicate two additional devals south of the 8.61°N deval, but those are not recognized by the chemistry with the present sampling frequency.

The third large segment, C, between the 9.06°N OSC and the Clipperton Fracture zone, has five devals of which two (at 9.63°N and 9.93°N) mark the separation of different clusters in isotope composition space. In general, the $^{208}Pb/^{204}Pb$ and $^{206}Pb/^{204}Pb$ in this segment continue the trend of decreasing values toward the north from the segment to its south (Figures 6b, 6c, and S1) and in Pb-Nd isotope space the samples from the segment between the 9.06°N OSC and Clipperton are distinct from the segments to the north and south (Figures 6c and S1). Twenty samples from the subsegment between 9.63°N and 9.93°N show a very limited range in Pb isotopic composition, and few of the samples fall outside the cluster toward more radiogenic Pb isotopic compositions. The samples between 9.93°N and the Clipperton Fracture Zone cluster at different Pb isotopic composition than the subsegment just to the south or samples north of the Clipperton Fracture Zone. This clustering is also observed in incompatible trace element ratios. Figures 4b and 4c shows this clustering clearly in Sr-Nd-Pb isotope space where the most radiogenic Pb samples are from south of the 9.06°N OSC and north of Clipperton.

Samples from the segment between Clipperton and the 11.75°N OSC (segment D) form two clusters with a deval at 11.09°N separating them. The clusters are easily recognized in Sr-Nd or Sr-Hf isotope space (see Figure 6d). The samples immediately north of the 11.75°N OSC (segment E) form a cluster separate from the segment to the south of it (see Figure 6f). North of the deval at 12.67°N (segment E2), the samples are not as tightly grouped as for the segments to the south. But from south of the Clipperton Fracture Zone

Figure 6d). The samples immediately north of the 11.75°N OSC (segment E) form a cluster separate from the segment to the south of it (see Figure 6f). North of the deval at 12.67°N (segment E2), the samples are not as tightly grouped as for the segments to the south. But from south of the Clipperton Fracture Zone

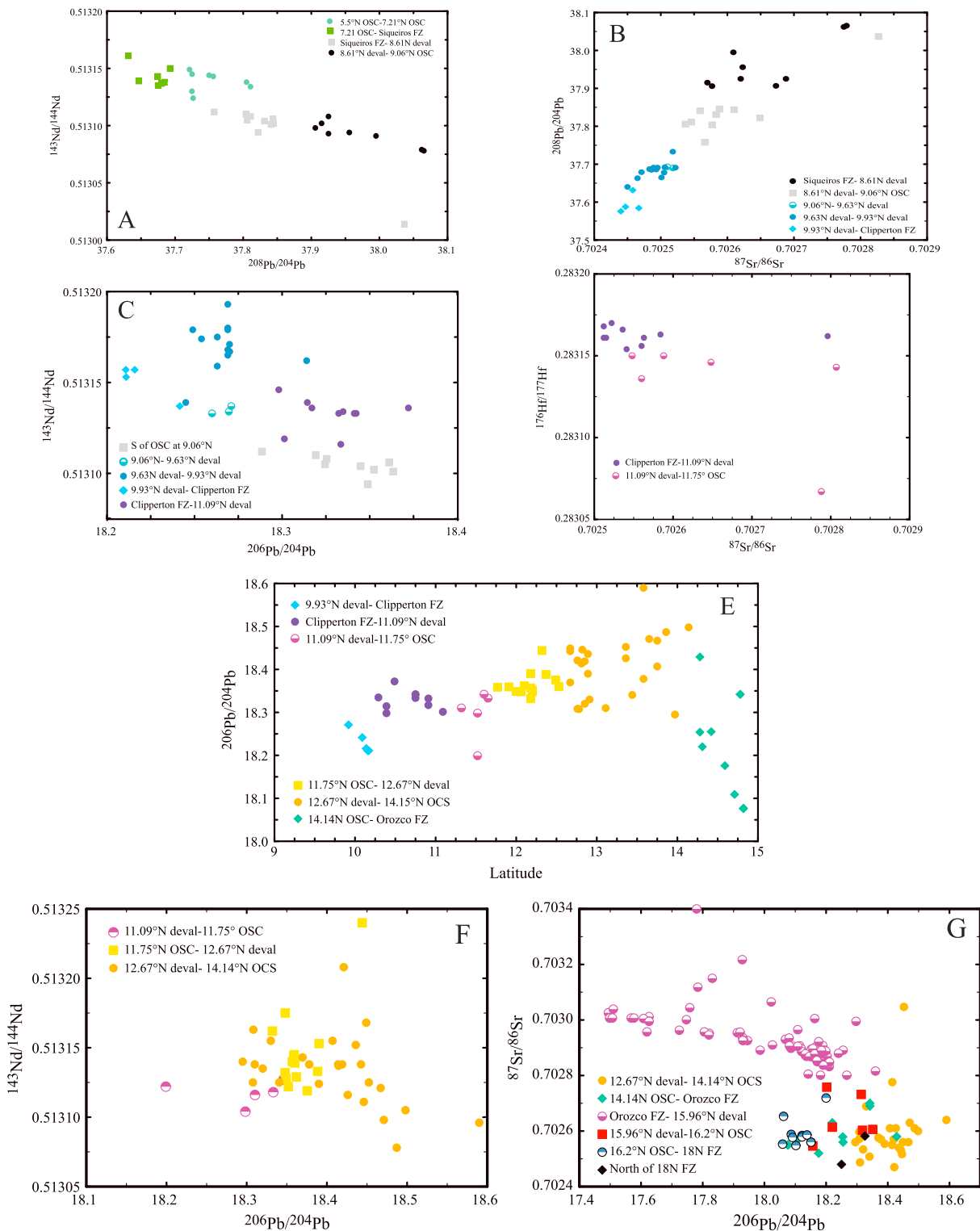


Figure 6. Variations in isotopic composition that show the clustering of chemistry of individual segments based on chemistry. Symbols as in Figure 2. Panels from A to G display segments successive segment going northward. A. Segments A and B north and south of the Siqueiros Transform Zone can be identified based on $^{208}\text{Pb}/^{204}\text{Pb}$ and $^{143}\text{Nd}/^{144}\text{Nd}$ isotopic composition. Both segments can be further subdivided with chemistry changing across the 7.21°OSC and the 8.61°N deval. B. Change in chemistry across the 9.06°N overlapping spreading center. Decreasing $^{208}\text{Pb}/^{204}\text{Pb}$ and decreasing $^{87}\text{Sr}/^{86}\text{Sr}$ through segments B and C. Segment C can be subdivided by devals at 9.63°N and 9.93°N. C. Change in chemistry across the Clipperton Fracture zone. D. Subdivision within segment D at the 11.09°N deval. E. Continuous increase in $^{206}\text{Pb}/^{204}\text{Pb}$ from 10°N to 14°N. F. Change in chemistry across the 11.75°N OSC. G. Clustering of adjacent segments with separate chemistry in the northern part of the study area. Adjacent segments have distinct isotopic compositions.

until the 14.14°N OSC (segment D and E) there is a clear gradient in $^{206}\text{Pb}/^{204}\text{Pb}$ isotopic composition with it becoming increasingly radiogenic to the north (see Figure 6e). Across the 14.14°N OSC there is a decrease in $^{206}\text{Pb}/^{204}\text{Pb}$ (see Figure 6e) to the north in samples from segment F.

The segment between the Orozco Fracture Zone and the 16.28°N OSC (segment G) is compositionally unlike any other part of the EPR and has radiogenic Sr and unradiogenic Pb, Nd, and Hf (see Figure 4f). This segment is characterized by a detailed study of Mougél et al. (2014). Samples with the most extreme isotopic compositions also have clearly distinct trace element composition (see section 6.3). Compared to its neighboring segments, this segment has a low mantle Bouguer anomaly that may indicate thickened crust and increased magma production (Carbotte et al., 2015). The northern boundary of this compositional “flavor” is sharp and occurs at the Deval at 15.96°N (see Figure 4f). The amount of data north of the 16.28°N OSC (segment H) is relatively limited, but the segment directly north of 16.28°N is isotopically distinct from the segment to its south and has more radiogenic Nd and Hf and less radiogenic Pb compared to the segment to its south (see Figure 4f).

The difference between adjacent segments is not restricted to the isotopic compositions but is often also observed with incompatible trace element ratios such as Ba/Th and La/Th, although the clustering of the trace element ratios is less clear. The chemical segmentation persists when plotted in three-dimensional space. In such diagrams that we present as movies S1 and S2 (supporting information), each ridge segment has limited overlap with its neighboring segments. In $^{206}\text{Pb}/^{204}\text{Pb}$ versus $^{207}\text{Pb}/^{204}\text{Pb}$ space adjacent ridge segments occupy different locations on this diagram or have different slopes. The difference in slope requires a change in at least one of the source components.

It is thus clear from this regional survey that there are variations in isotope values across ridge discontinuities at all scales. Every transform and large offset OSC shows a discontinuous change in isotopic composition, and some third- and fourth-order discontinuities demonstrate these changes as well. Magmatic segmentation in isotope values shows that the changes are not only occurring in the crust but also extending to source compositions.

6.2.1. Importance of Geological and Temporal Variability

The occurrence of these regularities is surprising in view of high-resolution geological studies that have taken place on both the northern and southern East Pacific Rise. Careful near-bottom studies have shown that lava flows can flow across a Deval (Goss et al., 2010; Bergmanis et al. 2007). In this case any variations that might have been organized with respect to the smallest scales of segmentation would be obscured. Indeed, lava flows have been mapped to extend up to 15 km along axis (J. Sinton et al., 2002), which would cause boundaries to be diffuse rather than sharp. Bergmanis et al. (2007), however, conclude that most flow of lava is vertical and that ordinarily lateral movement along axis is limited in cases such as the East Pacific Rise where magma supply from the mantle is more or less continuous along strike. Where there is a point source of magma, such as in Hawaii, dikes may propagate large distances carrying magma from the point source along a rift zone. But where there is a continuous supply of magma, the crack may propagate but nonetheless be filled largely from magma below. In this case, even single eruptive episodes might preserve discontinuities in composition along strike. It is also noteworthy that along the southern EPR, large offset OSCs (e.g., 20° 30' S) are also sites of abrupt steps in chemical composition.

Bergmanis et al. (2007) also note that the importance of temporal variation where older lava flows, still exposed near the axis, tends to be of a more enriched composition. The temporal extent of variations is virtually unexplored terrain that would require extensive time series data at the same scale as zero age sampling (e.g., see Ferguson et al. 2017)—a daunting task.

6.3. Significance of Isotopic Contrasts Across Segment Boundaries

There are many other locations along the ridge system where ridge offsets correspond with discontinuities in chemistry (e.g., Langmuir & Bender, 1984) including isotopic composition. These include the Chile Ridge in the Pacific (Sturm et al., 1999), east of the Prince Edward Fracture Zone in the Indian Ocean basin (Meyzen et al., 2005), the Kane Fracture Zone (Machado et al., 1982), the Menard Transform Zone (Hamelin et al., 2010), the Hayes Transform Zone (Smith et al., 1998), the propagating rifts that bound the Galapagos hot spot (Ingle et al., 2010; Schilling et al., 2003; Sinton et al., 2003), the Australian Antarctic Discordance (Hanan et al., 2004; Klein et al., 1988), the north Atlantic at the Gibbs, Tjörnes

and Jan Mayen Fracture Zone (Blichert-Toft et al., 2005; Schilling et al., 1999), as well as subaerial Iceland (Shorttle et al., 2013). In the southern EPR the second-order discontinuity at 20°30'S also is a major boundary (Mahoney et al., 1994). These are all major offsets that generally also correspond with marked changes in the depth of ridge axis and thus would seem to be reflecting larger-scale characteristics of mantle flow or composition. What is novel in the present study is the high resolution of the data that demonstrates the existence of discrete isotopic clusters of composition on very short length scales and across ridge offsets that include not only transform faults and large offsets OSCs but also the small offset third- and fourth-order discontinuities (devals).

How can spatial variability of heterogeneity in the subridge mantle be preserved during melt transport and ponding in a magma lens? The observed magmatic segmentation indicates that there is limited lateral flow and mixing in crustal magma chambers even where there is a subaxial magma lens. This supports the “multiple supply” model of continuous magma input along axis even in the presence of an axial magma body (Langmuir, 1987; Langmuir et al., 1986), a conclusion also reached by Bergmanis et al (2007) for their studied portion of the southern EPR.

The gradient in isotopic composition as is observed in Figure 4e also shows a larger wavelength heterogeneity than the magmatic segmentation. If there is an existing ridge, parallel gradient in isotopic composition of the subridge mantle and individual ridge segments average out melts from a subset of the gradient then these averages will have distinct compositions. This process could be partly responsible for the clustering of the isotopic compositions. It would imply that even melts from deeper reaches of the melt regime would consistently aggregate at the same side of a discontinuity and that transport across a plane extending from a discontinuity is minimal. Additionally at many locations in our study area the clustering is such that there is almost complete separation between segments and minimal overlap. This suggests that the location of the discontinuity may at least in part be a consequence of differences in source composition.

The mechanism that would couple source composition with surface tectonics is most likely related to physical differences of the sources. At this section of the EPR the source seems to consist of three components (see discussion below); each most likely has a different solidus and different melting behavior. The limited variation in ridge depth indicates that the potential temperature variations along the ridge are limited and that the mantle below the EPR follows the same P-T path before melting starts. However, the different mixtures of the three components will have different solidi and different melting rates. The solidus of peridotite alone can vary by about 100 K dependent on its fertility (Hirschmann, 2000). If different lithologies are considered, the difference in solidus temperature can be even larger. With an enthalpy of melting of about $600 \text{ J}\cdot\text{g}^{-1}$ and a specific heat of $1.0\text{--}1.5 \text{ J}\cdot\text{g}^{-1}\cdot\text{K}^{-1}$, the difference in solidus temperature will quickly result in fairly large temperature gradients; that is, the differences in solidus temperature become the difference in the ambient temperature of the mantle. Thermal diffusivity is not fast enough to eradicate the temperature difference; over 1 Myr differences in temperature over a distance of approximately 20 km can be eradicated, but larger-scale gradients will persist longer. Thus, the compositional differences at depth will be translated in temperature differences at shallower depths in the melting regime. Water content is an important control on the mantle viscosity and mantle flow beneath the ridge (Hirth & Kohlstedt, 1996). Since water behaves similar to Ce during melting (Michael, 1988; Saal et al., 2002), the different onsets of melting will result in variations in water content even if water contents were initially uniform. The removal of water and the decrease in temperature both will increase the viscosity of the residue. A natural “break” in physical parameters occurs where the contrast between chemical compositions is largest. Both variations in chemical composition and the distribution of heterogeneities can affect the physical parameters of the mantle such as temperature and viscosity and, in turn, affect segmentation.

It is easy to envisage that differences in solidus with associated differences in temperature, magma production, and rheology can have an influence on the location of second- or higher-order discontinuities. These are more transient features that can move along the ridge or disappear. However, first-order discontinuities can be hundreds of kilometers in length; the Clipperton FZ can be traced for over 1,000 km. If the chemical differences persist over such a distance, it would imply large length-scale consistent variations with a relatively sharp transition between two mantle compositions. Linear-type features are observed at Hawai'i where the difference between Loa and Kea trend on Hawai'i persists on the surface for at least 400 km

Table 1
Composition of the Proposed Three Endmembers

Parameter	Depleted	Gabbro	Enriched
Sr	80	186.8	260
Nd	3	15.534	14.5
Pb	0.1	0.228	1.1
Rb	0.2	0.124	17
La	1.63	1.7	7
Ce	5.9	12.362	34
Ba	1	17	100
TH	0.05	0.096	0.75
U	0.01	0.026	0.417
Nb	0.85	1.5	14
Yb	2.68	5.62	2
$^{87}\text{Sr}/^{86}\text{Sr}$	0.7023	0.703125	0.7029
$^{143}\text{Nd}/^{144}\text{Nd}$	0.513289	0.51303	0.51297
$^{206}\text{Pb}/^{204}\text{Pb}$	18.2	17.4	19
$^{207}\text{Pb}/^{204}\text{Pb}$	15.36	15.47	15.6

(Weis et al., 2011) and exceeds the length of many fracture zones. There are also two parallel trends of volcanoes of distinct isotopic composition at the Society Islands extending for approximately 400 km (Payne et al., 2013). Whether the geochemical differences on either side of a first-order discontinuity persist in older crust is unknown as there are to our knowledge only two studies that investigated the temporal variation in composition for a significant length off-ridge. Similar isotopic compositions of basalts up to 50 km (800 kyr) from the ridge axis was observed at 9 N on the EPR (Regelous et al., 1999). A study of the temporal variation at the VEMA fracture zone shows that the Sr and Nd isotopic composition of the basaltic crust on the south side of the fracture zone is essentially constant over the length of the study area (350 km representing about 20 Ma; Cipriani et al., 2004).

6.3.1. Complexities of Sampling the Melting Regime

Rudge et al. (2013) and Shimizu et al. (2016) have recently suggested that complex mixing in the melting region can produce a diversity of trace element and isotope compositions by independent melting of two lithologically independent sources.

In essence, a pyroxenite lithology begins to melt at greater depth, and these melts mix with shallower melts of peridotite as the pyroxenite also continues melting to the surface. Because both lithologies melt fractionally, and fractional melting affects the trace elements to an extreme while not affecting the isotopes, a huge diversity of trace element compositions is produced for each separate isotopic composition. The individual melts then form two large vertical linear arrays on plots of an incompatible element ratio (x) versus an isotope ratio (y), and diverse mixtures of these melts can then create a box of compositions that have little relevance to the source compositions. Depending on the way these diverse melts are mixed, complex and nonintuitive results can be produced, including chemical arrays that are derived from two components that appear to reflect three components or linear arrays that do not extend to the endmember isotopic compositions. While this model has mathematical appeal, the question is whether the process proposed occurs in the mantle, and if so how one might distinguish it from more conventional interpretations of mixing of endmembers.

We are using the basalt compositions to determine endmember melt composition that mix to form the chemical variations. It should be understood that these melt compositions are sampling a source, but there is a potential bias in this sampling as the isotopic compositions and trace element ratios can reflect an incomplete sampling of the source (Salters & Dick, 2002; Stracke et al., 2011). How the mantle is sampled and how the melts are transported can potentially effect the composition of the melts (Rudge et al., 2005; Shorttle & MacLennan, 2011; Stracke & Bourdon, 2009). The question then is whether the differences between segments relate to differences in source composition or are they related to differences in the way sources are melted and sampled before eruption.

The first important aspect is that these complexities proposed by Rudge et al. (2013) do not occur for Pb isotopes. The Pb isotopes still reflect the mixing endmembers. Since the Pb isotope data alone in this study region require three components, it is evident that the conclusion of three endmembers is not an artifact of complex mixing of melts in the mantle.

Rudge et al. (2013) propose that there is efficient mixing of pyroxenite and peridotite sources below 85 km and that this intermediate composition then forms a kind of mixing endmember with shallow fractional melts of pyroxenite and peridotite. In this case one would predict a common enriched member for all the segments. However, this is not observed. The Pb isotopes are particularly significant in this regard as the individual ridge segments have different slopes in $^{206}\text{Pb}/^{204}\text{Pb}$ - $^{207}\text{Pb}/^{204}\text{Pb}$ space indicating a different mix of source components for the individual segments.

There are other tests of the Rudge et al. (2013) model. For low values of their mixing parameter (N), there should be no correlation between incompatible element contents and isotope ratios. Such correlations, however, are present in the EPR data. For high values of N (well-mixed melts), correlations reappear with Nd isotopes but only at the expense of greatly damping the total variance of both trace elements and isotopes. The EPR data show large variations in incompatible element concentrations, inconsistent with large

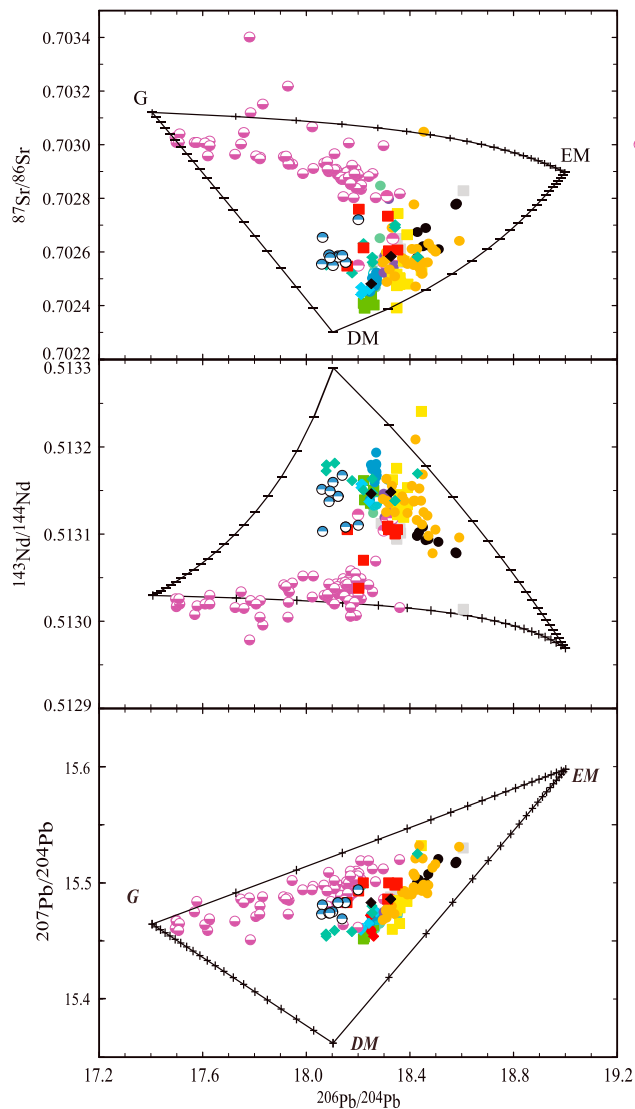


Figure 7. Mixing calculations for the three chosen endmembers in isotopic composition space. G is gabbroic component, DM is depleted mantle, and EM is enriched mantle. Symbols as in Figure 2. Tick marks at mixing curves are 5% increments of a component.

composition and share chemical characteristics (Niu et al., 2002) although the off-axis seamount basalts are more heterogeneous than the N-EPR ridge basalts (Brandl et al., 2012; Fornari et al., 1988; Graham et al., 1988; Niu & Batiza, 1997; Niu & O'Hara, 2008; Shimizu et al., 2016; Zhang et al., 2016; Zindler et al., 1984). It has been argued that seamount basalts, by nature of their relatively small volume, faithfully reflect the source heterogeneity of the subridge EPR mantle, and the majority of the geochemical variability of the lavas that erupted in the N-EPR region is controlled by a two-component mantle: an enriched and low solidus component and one depleted in incompatible elements (Fornari et al., 1988; Graham et al., 1988; Niu & Batiza, 1997; Niu & O'Hara, 2008; Zindler et al., 1984). A cursory look of the N-EPR ridge basalt chemistry shows overlap with the seamount basalt chemistry, but compositional trends of MORB particularly from segment G, north of the Orozco Transform, require a third component (see Figure 3b). While the variations in Sr, Nd, and Hf isotope ratios of EPR basalts are similar to those of the seamount basalts, individual segments show overlapping variations with a different slopes which excludes mixing of just one enriched and one depleted component and indicates the presence of a third component. The presence of an additional component becomes very evident in compositional space that includes the Pb isotopes (Figure 3). For example, in

values of N . Furthermore, their reported model results show no correlations between highly incompatible elements and Pb isotopes, and the EPR data show quite good correlations.

Chemical variation can also be created during magma transport between point of origin and eruption by reactive melt transport (Spiegelman & Kelemen, 2003; Katz & Weatherley, 2012). However, melt transport cannot create isotopic variation. Thus, to explain the variation in the basalts still requires three components; the question becomes whether some of the variations between ridges can be explained by variations in reactive melt transport as opposed to source variations. Trace element variations as the result of reactive porous flow as opposed those from source variation are difficult to distinguish. The range in trace element variations that can be created is largest for the highly incompatible elements. Therefore, one would not expect correlations between isotopic composition and incompatible trace element ratios, and the data in fact are well correlated.

Therefore, there is no aspect of the EPR data that supports the complexities of chemical transport nor the fractional mixing process that Rudge et al. (2013) propose. Why would this be? The Rudge et al. (2013) model requires separation of sources at depth and complete separation of pyroxenite melts from peridotite melts at all depths above 85 km. This requires large and physically separate pyroxenite bodies on the scale of tens to hundreds of meters or more. It is possible that the heterogeneities are on a smaller scale, which permits mixing of melts within the melting column rather than completely separate melting regimes for the two lithologies as they model. If low degree melts are the origin of the heterogeneities (e.g., Donnelly et al, 2004), then enriched domains lie along grain boundaries. If melts are always of peridotite, some peridotites have higher incompatible element concentrations owing to a larger proportion of the low-degree melt component. Mixing then takes place in the source region of a single lithology, albeit with different volatiles contents that may influence the onset of melting. In this case, a classical approach to mixing endmembers remains appropriate and is not complexified by physically separated lithologies.

6.4. Compositional Trends and Mixing Relationships

The large range in incompatible trace element ratios and isotopic compositions clearly indicates the mantle source beneath the N-EPR is heterogeneous. The ridge basalts and off-axis seamount basalts also overlap in

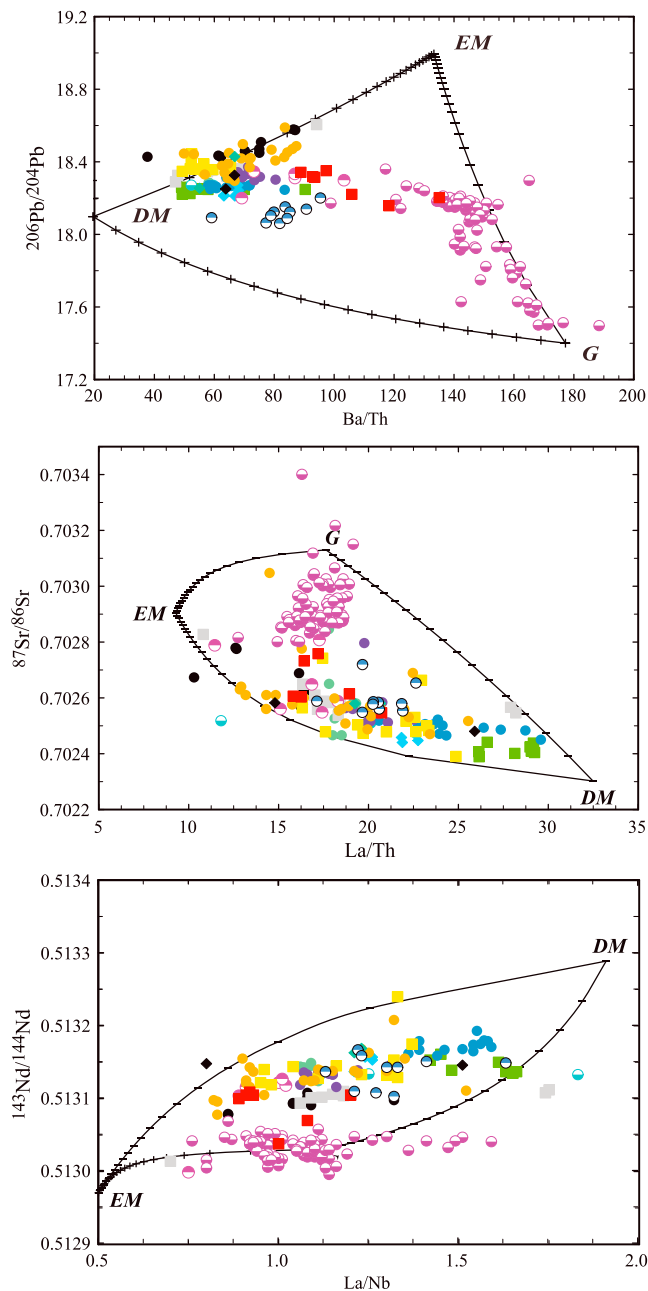


Figure 8. Mixing calculation on isotopic composition versus incompatible element ratio showing that the compositional range at the EPR can be explained by three component mixing. Tick marks at mixing curves are 5% increments of a component. Symbols as in Figure 2.

(Niu et al., 2002), and a composition similar to the seamount basalts is taken as the enriched component. Endmember compositions are listed in Table 1 and shown in Figures 7 and 8. The estimated enriched and depleted endmember compositions are similar to the endmember compositions proposed in the other studies (Castillo et al., 2000; Donnelly, 2002; Lundstrom et al., 1999; Niu et al., 2002). Waters et al. (2011) based on U-Th disequilibria, trace elemental and isotopic compositions, argued that the chemical variation at the 9–10°N is due to mixing of melts from different sources as opposed to mixed sources which subsequently melt. However, it should be noted that this modeling solution is nonunique. The lack of correlation of major elements such as Na₈ or CaO/Al₂O₃ with isotopic compositions also indicates that melts from different stages of melting and/or fractional crystallization are mixed.

²⁰⁶Pb/²⁰⁴Pb versus ¹⁴³Nd/¹⁴⁴Nd (and ²⁰⁶Pb/²⁰⁴Pb vs. ⁸⁷Sr/⁸⁶Sr) diagrams segment G displays a compositional trend with significantly different slope than the other ridge segments. The ⁸⁷Sr/⁸⁶Sr-²⁰⁶Pb/²⁰⁴Pb variations also show a range in Sr-isotope composition for given ²⁰⁶Pb/²⁰⁴Pb isotope ratio that requires more than two components.

Three-component mixing calculations can reveal whether three components could explain all the variations. We choose (1) a depleted component—depleted in incompatible elements and with radiogenic Nd, Hf, and unradiogenic Sr and Pb; (2) an enriched component—enriched in incompatible elements and with unradiogenic Nd, Hf, and radiogenic Sr and Pb; and (3) a component modeled after a gabbroic composition with unradiogenic Nd, Hf, ²⁰⁶Pb/²⁰⁴Pb, and ²⁰⁸Pb/²⁰⁴Pb with comparatively high concentrations of Ba (high Ba/Nb, Ba/Zr, and Sr/Nd; a positive Eu-anomaly; low Ce/Pb and low La/Sm and relatively high ⁸⁷Sr/⁸⁶Sr; and a high U/Pb ratio). The basalts with the least radiogenic Pb isotopic compositions also have high Al₂O₃ content and positive Eu-anomaly (Donnelly, 2002; Mougel et al., 2014) indicating the presence of abundant plagioclase and their ancient origin. The high abundance of plagioclase is consistent with the low Ce/Pb and U/Pb the latter resulting in low ²⁰⁶Pb/²⁰⁴Pb isotopic compositions. As noticed by Donnelly (2002) and Mougel et al. (2014, 2015) this component is different than any of the named mantle endmembers; they argue for a metagabbroic pyroxenite.

We used a gabbro composition similar to that reported by Hart et al. (1999) and Zimmer et al. (1995). The isotopic composition of this component is similar to that of a 1.7-Ga gabbro from oceanic crust that has been modified during subduction (Stracke, Bizimis, et al., 2003), and we call this a metagabbro and assume an eclogitic/pyroxenitic lithology, that is, it has been subducted and recycled deep into the mantle and amphibole is absent. The absolute concentrations of trace elements of a melt from this bulk composition are poorly constrained and somewhat arbitrary. The temperature difference between the solidus and liquidus of a gabbro is small, and as long as there is no residual garnet the bulk gabbro and the melt will be relatively similar. The absence of fractionation of the LREE from the HREE indicates that there is no residual garnet and that the magmas derived from this component represent a relatively large degree of melting (Mougel et al., 2014). Concentrations that are twice that of the modified gabbro are used in the simple melt mixing calculations.

The initial choices for the other components are relatively obvious. For the depleted component we used the depleted basalts from the Garrett Transform Fault at the south EPR (Wendt et al., 1999), which in terms of trace elements and isotopes are the most depleted of the EPR. Off-axis seamount basalts are the most enriched basalts of this part of the Pacific

Table 2
Loadings of the Chemical Parameters on the Principle Components

Parameter	PC1	PC2	PC3	PC4	PC5
$^{87}\text{Sr}/^{86}\text{Sr}$	0.286	-0.156	0.046	-0.001	0.116
$^{143}\text{Nd}/^{144}\text{Nd}$	-0.295	0.139	0.064	0.143	0.126
$^{206}\text{Pb}/^{204}\text{Pb}$	-0.048	0.516	0.114	-0.166	-0.020
$^{207}\text{Pb}/^{204}\text{Pb}$	0.192	0.313	0.065	-0.335	0.459
$^{208}\text{Pb}/^{204}\text{Pb}$	-0.060	0.519	0.080	-0.156	0.104
Ba/Th	0.290	-0.280	0.020	-0.053	0.112
Th/U	0.258	0.148	-0.024	0.372	0.527
Ba/La	0.347	-0.119	-0.059	0.015	-0.005
La/Th	-0.310	-0.166	-0.002	-0.364	0.028
Nb/Th	-0.117	-0.128	0.891	0.065	-0.089
La/Nb	-0.290	-0.139	-0.316	-0.430	0.052
Sr/Nd	0.141	-0.279	0.246	-0.508	0.349
Ce/Yb	0.300	0.160	0.077	-0.231	-0.428
La/Sm	0.304	0.202	0.016	-0.179	-0.354
Ba/Zr	0.348	-0.032	-0.075	-0.089	-0.130
Percentage	51.11	22.68	6.68	5.49	4.81
Cumulative percentage	51.11	73.79	80.47	85.96	90.77

Mixing calculations using Table 1 endmembers reproduce the general trends and most of the compositional variation in trace element and isotope ratios. The variations displayed by the basalts all fall internal to the field defined by the proposed components and the mixing lines between them. Note that no segment represents mixing between pure components (see $^{206}\text{Pb}/^{204}\text{Pb}$ vs. $^{87}\text{Sr}/^{86}\text{Sr}$ and $^{206}\text{Pb}/^{204}\text{Pb}$ vs. $^{143}\text{Nd}/^{144}\text{Nd}$; Figure 7). It is also important to note that the majority of the samples contain a large amount of the depleted component. It implies that the depleted mantle plays the major role in controlling the composition, but all three components are present under all segments and are sampled to different degrees. The presence of the gabbro component is well shown in the $^{206}\text{Pb}/^{204}\text{Pb}$ versus $^{143}\text{Nd}/^{144}\text{Nd}$ variation where the gabbro component is extremely obvious for the samples from the G1 segment and also for segment G2, H, and F. For the latter three even if the two other endmembers are changed to less radiogenic $^{206}\text{Pb}/^{204}\text{Pb}$ compositions the three segments deviate in $^{206}\text{Pb}/^{204}\text{Pb}$ for given $^{143}\text{Nd}/^{144}\text{Nd}$ from the trend formed by the other segments (excluding G1) that a third component is needed.

Principal component analysis using 15 parameters was used in this analysis: Ba/Th, Th/U, Ba/La, La/Th, Nb/Th, La/Nb, Sr/Nd, Ce/Yb, La/Sm, Ba/Zr as well as the Sr, Nd, and Pb isotopic compositions reveal that two components can explain 74% of the observed variation and this is consistent with the elongated trends observed for the individual ridge segments. In order to investigate whether the principle component analyses was dominated by the large data set on the relatively small segment G2 with the strongly deviating Pb isotopic composition, we did the analysis both with and without the data of the Moguel et al (2014). There was no significant difference in the loadings on the principle components nor was there a significant change in the number of components needed to explain the data.

Two components are explained by PC1 in Table 2 and have significant loadings for all parameters except for the Pb isotopic composition and Nb/Th and Sr/Nd and explain 51% of the variation. With a positive loading for $^{87}\text{Sr}/^{86}\text{Sr}$ and a negative for $^{143}\text{Nd}/^{144}\text{Nd}$ PC1 is related to the enrichment depletion that gives rise to the negative correlation between Sr and Nd isotopic compositions and levels of enrichment in the mantle. PC2 has the highest loading for the Pb isotopic composition and explains another 23% of the observed variations. The loadings of the parameters on the components are in Table 2, and the loadings of the first three components are in Figure 9. Samples from segment H, F, and G1 and G2 have significant loadings of PC2 indicating that the gabbro-like component is present. PC2 represents a significant part of the variation of all samples, indicating that the gabbroic component is ubiquitous beneath the EPR. This is especially clear in Sr-Nd-Pb isotope space and Nd-Pb isotope, Ba/Th space (see movies in supporting information). Another 17% of the variation can be explained by an additional three components. Parameters sensitive to source and crystal fractionation or melting like La/Sm, Ba/Zr, and Ce/Yb do not require a separate component; that is, they are correlated with the isotopes. This indicates that source processes as opposed to

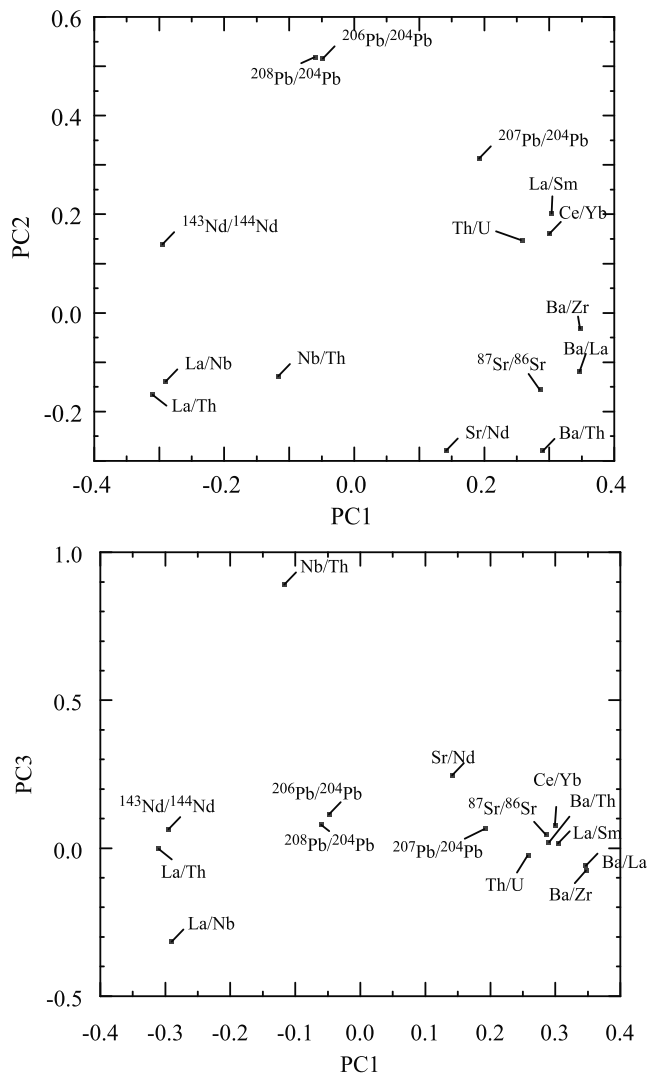


Figure 9. Loadings of the parameters on the first three principle components.

fractionation processes dominate the variations. The highest loading for components 3, 4, and 5 is Nb/Th, Sr/Nd, and U/Th, respectively, and the loadings are heavily weighted toward just one chemical parameter and as such do not identify individual mantle components but more the variability of the individual components.

The compositional variation of individual ridge segments is often more linear creating the impression that only two endmembers are present. These two endmembers at the segment scale are both a mixture of the three components. Waters et al. (2011) suggest that two components explain most of the variation in the 9–10°N on-axis basalts but that Pb isotope variation in off-axis E-MORB and in our data shows that this segment (C) looks like binary mixing with a relatively small amount of the gabbro-like component. Donnelly (2002) also proposed similar three-component mantle to explain the chemical variability in the Orozco region. It is also important to consider that on a $^{206}\text{Pb}/^{204}\text{Pb}$ versus $^{207}\text{Pb}/^{204}\text{Pb}$ diagram different segments have different slopes (see Figure 3). Especially segments E1 and E2, F and G1 have different slopes from the main trend. This indicates the presence of at least three components.

Earlier studies have argued that the subridge mantle at the EPR is variably polluted by a low-solidus enriched component (Castillo et al., 2000; Lundstrom et al., 1999; Niu & Batiza, 1997; Zindler et al., 1984), and this could explain the E-MORB and off-axis seamounts. Waters et al. (2011) argued, based on the enriched trace element character of the E-MORB from the 9–10°N EPR and their larger ^{230}Th excesses than N-MORB, that these E-MORBs are a mixture of an early melting component from a garnet pyroxenite and a shallow melt from a peridotite-pyroxenite source. If the enriched component would be an enriched lithology such as pyroxenite or eclogite, then the major element composition of the melts from the enriched lithology, like SiO_2 and $\text{CaO}/\text{Al}_2\text{O}_3$, would be noticeably different (Hauri, 1996; Pertermann et al., 2004; Pertermann & Hirschmann, 2003). However, trace element ratios and isotope ratios do not correlate with Na_8 (at the segment level or as a whole) or with other major elements. The ^{230}Th excesses of E-MORB, however, require melting in the presence of garnet. Donnelly (2002) explains E-MORB by melting of metasomatized peridotite but to relatively small amount and in the spinel stability field and no residual garnet.

Trace element ratios display relatively coherent variation with isotope ratios (Figure 10). Incompatible element-enriched basalts (samples with higher Ba/La, Ba/Zr, and Sm/Yb) display unradiogenic Nd and Hf and radiogenic Sr and Pb isotope ratios. The incompatible element enrichment could be either an enriched source or a low degree melt; the isotope and trace element ratios with isotope ratios are consistent with E-MORBs preferentially sampling radiogenic Sr-Pb and unradiogenic Nd-Hf compositions of either a trace element enriched source or a low degree of melting.

Stracke and Bourdon (2009) argued that the incompatibility of Ba, La, and Sr is significantly different in peridotite versus pyroxenite. Pyroxenite melts will have lower Ba/Th and La/Nb and higher Sr/Nd than a peridotite-derived melt. The enriched component in this study has low La/Nb but high Ba/Th and low Sr/Nd, inconsistent with a pyroxenite lithology and an enriched source as chosen by Stracke and Bourdon (2009). Thus, if the enriched component is pyroxenitic, then its source will need to have even higher Ba/Th and lower Sr/Nd than calculated as the endmember composition, which is not likely. Therefore, our preferred model would be an enriched peridotitic source for the enriched component. In this case though the ^{230}Th excesses require the enriched (metasomatized) peridotite to start melting in the garnet stability field and thus represent a high degree of melting. To generate an E-MORB from a

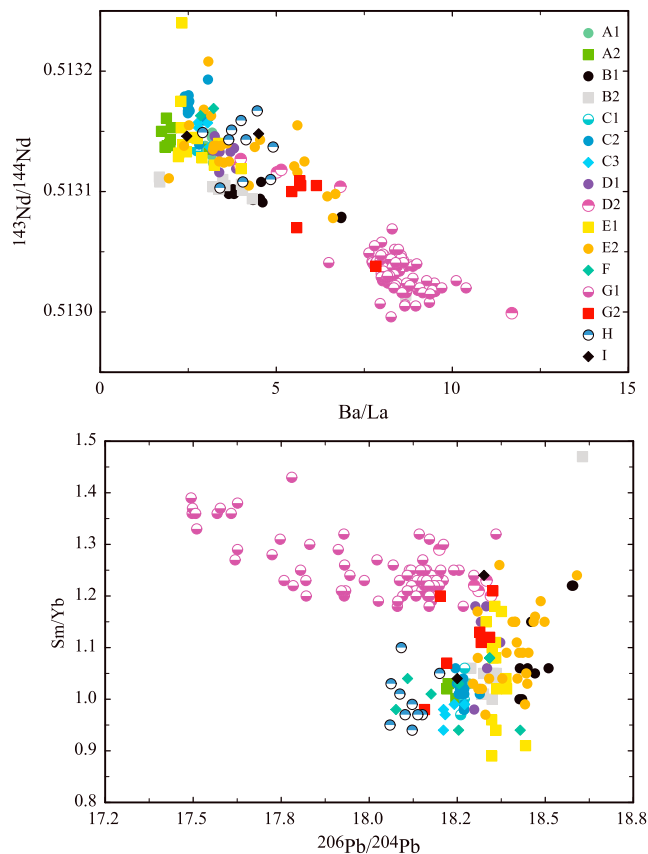


Figure 10. Incompatible trace element ratios versus isotopic composition showing that these parameters are correlated in a broad sense.

peridotite that undergoes a large degree of melting requires the peridotite to be more enriched than if the E-MORB represents a low degree of melting. That raises the question whether this enrichment is then still compatible with the E-MORB isotopic compositions in a reasonable time frame. The study by Donnelly (2002) suggests based on the correlations between isotopic compositions and parent-daughter ratios that the E-MORB source is several hundreds of millions years but less than 1 Ga old.

We used the most enriched E-MORB (CH75-1) from segment B2 to calculate the age of the metasomatism if CH75-1 represents a large degree of melting. We calculated the potential source of CH75-1 if it represents a melt of more than 5% melting of which part took place in the garnet stability field. We used the melting models and partition coefficients of Salters and Longhi (1999) and Salters et al. (2002). We can then calculate the age of that source with the isotopic composition of CH75-1. Its isotopic compositions dictate that prior to being metasomatized the peridotite has to have been depleted relative to bulk silicate Earth. We used a three-stage evolution model with bulk silicate earth, depleted mantle, and metasomatized mantle. The composition of the depleted mantle was taken from Salters and Stracke (2004) with a 2-Ga age. The intersection of this evolution line with that of the calculated metasomatized source yielded the age of metasomatism. The calculations show that metasomatized peridotite can yield lavas like CH75-1 by 10–15% melting of which a portion, 20–30%, of the melting took place in the garnet stability field with the bulk of the melting in the spinel peridotite field with the age of metasomatism more than 200 Ma but less than 1 Ga. The Rb/Sr isotope system consistently has a younger age compared to the Hf-Nd and Pb system. This younger age is attributed to the somewhat fractionated nature of CH75-1 with a Mg# of 0.5 and 5.62 wt.% MgO. Thus, the Sr

concentration could have been lowered by plagioclase fractionation, resulting in a higher Rb/Sr and consequently higher Rb/Sr for the calculated source and thus younger age. This calculation does not exclude pyroxenite as contributing to the E-MORB but indicates a metasomatized peridotite. Given these calculations and the high Ba/Th and low Sr/Nd, we prefer a metasomatized garnet peridotite as the source for E-MORB.

It has been proposed that trace element variations and fractionations can be enhanced during melt transport by reaction of the melt with the matrix it is traveling through. (Spiegelman & Kelemen, 2003). There are several lines of argument against this process being responsible for the trace element variations. The first line of evidence is the correlation between the trace elements and the isotopic compositions. The second line of evidence comes from the nature of the trace element variations. For example, to explain the range in Ba/Th by dynamic melting, the accompanying trace element concentration is much larger than the observed concentration range for either Ba or Th. Since the trace element variation requires different components, there is also no need to call on these melt transport processes to further fractionate the trace elements, although the process cannot be completely excluded.

7. Conclusions

The following can be concluded with respect to magmatic processes and source composition at the northern East Pacific Rise:

1. Geochemical clustering coincides with the ridge discontinuities, even those with very small offsets. Correlation between the source related chemical characteristics and segmentation of the ridge crest implies that mantle composition is a factor influencing discontinuities. Variations in source composition or melting behavior are likely factors that influence segmentation. Geochemical observations are inconsistent with melt transport across the discontinuities.

2. Trace element variability correlates with isotopic variability and therefore is dominated by source processes. The correlations between incompatible element ratios and Sr contents, and the highly incompatible element behavior of Ba, demonstrate that the regional variations are derived from variations in source and extent of melting, not crustal magmatic processes.
3. Along-axis variation in MORB chemistry within a segment is consistent with melt transport being mostly vertical with limited along axis transport.
4. Recent models proposing melting of physically separated pyroxenite and peridotite lithologies are not consistent with the combined major element, trace element, and isotope variations.
5. Compositional variability can be explained by the presence of three endmembers—depleted mantle, enriched mantle, and recycled, ancient, and gabbro. The high-resolution sampling and analysis reveal that the each segment has a characteristic chemical signature, occupying different compositional space and/or displaying different trends. All three components contribute along this section of the East Pacific Rise. There is no evidence for recycled upper crust as a primary source component.

Acknowledgments

This work was supported by NSF grant OCE 0648484 to V. S. and various OCE grants to C. L. Constructive discussions with Mike Perfit improved this manuscript. Caitlyn Salters is thanked for help with sample preparation. Afi Sachi-Kocher is thanked for help with the chemistry at FSU; Zhongxing Chen is thanked for ICP-MS analyses at Harvard. The data used in this paper can be found as indicated either in the supporting information or in the references. John MacLennan, John Rudge, and several anonymous reviewers are thanked for their constructive review of this manuscript. A portion of this work was performed at the National High Magnetic Field Laboratory, which is supported by National Science Foundation Cooperative agreement DMR-1157490 and the State of Florida.

References

- Batiza, R., Niu, Y., Karsten, J. L., Boger, W., Potts, E., Norby, L., & Butler, R. (1996). Steady and non-steady state magma chambers below the East Pacific Rise. *Geophysical Research Letters*, *23*(3), 221–224. <https://doi.org/10.1029/95GL00016>
- Bender, J. F., Langmuir, C. H., & Hanson, G. N. (1984). Petrogenesis of basalt glasses from the Tamayo region, East Pacific Rise. *Journal of Petrology*, *25*(1), 213–254. <https://doi.org/10.1093/ptrology/25.1.213>
- Bergmanis, E. C., Sinton, J., & Rubin, K. H. (2007). Recent eruptive history and magma reservoir dynamics on the southern East Pacific Rise at 17°30' S. *Geochemistry, Geophysics, Geosystems*, *8*, Q12006. <https://doi.org/10.1029/2007GC001742>
- Blichert-Toft, J., Agraniér, A., Andres, M., Kingsley, R., Schilling, J. G., & Albarède, F. (2005). Geochemical segmentation of the Mid-Atlantic Ridge north of Iceland and ridge-hot spot interaction in the North Atlantic. *Geochemistry, Geophysics, Geosystems*, *6*, Q01E19. <https://doi.org/10.1029/2004GC000788>
- Brandl, P. A., Beier, C., Regelous, M., Abouchami, W., Haase, K. M., Garbe-Schönberg, D., & Galer, S. J. (2012). Volcanism on the flanks of the East Pacific Rise: Quantitative constraints on mantle heterogeneity and melting processes. *Chemical Geology*, *298*, 41–56.
- Canales, J. P., Carton, H., Carbotte, S. M., Mutter, J. C., Nedimovic, M., Xu, M., et al. (2012). Network of off-axis melt bodies at the East Pacific Rise. *Nature Geoscience*, *5*(4), 279–283. <https://doi.org/10.1038/NNGEO1377>
- Carbotte, S. M., & Macdonald, K. C. (1992). East Pacific Rise 8°–10°–30'N: Evolution of ridge segments and discontinuities from Seamount II and three-dimensional magnetic studies. *Journal of Geophysical Research*, *97*(B5), 6959–6982. <https://doi.org/10.1029/91JB03065>
- Carbotte, S. M., Marjanovic, M., Carton, H., Mutter, J. C., Canales, J. P., Nedimovic, M. R., et al. (2013). Fine-scale segmentation of the crustal magma reservoir beneath the East Pacific Rise. *Nature Geoscience*, *6*(10), 866–870. <https://doi.org/10.1038/ngeo1933>
- Carbotte, S. M., Mutter, M., Mutter, J., & Ponce-Correa (1998). Influence of magma supply and spreading rate on crustal magma bodies and emplacement of the extrusive layer: Insights from the East Pacific Rise at lat 16°N. *Geology*, *26*(5), 455–458. [https://doi.org/10.1130/0091-7613\(1998\)026<0455:IOMAS>2.3.CO;2](https://doi.org/10.1130/0091-7613(1998)026<0455:IOMAS>2.3.CO;2)
- Carbotte, S. M., Small, C., & Donnelly, K. (2004). The influence of ridge migration on the magmatic segmentation of mid-ocean ridges. *Nature*, *429*(6993), 743–746. <https://doi.org/10.1038/nature02652>
- Carbotte, S. M., Smith, D. K., Cannat, M., & Klein, E. M. (2015). Tectonic and magmatic segmentation of the Global Ocean Ridge System: A synthesis of observations. In T. J. Wright, A. Ayele, D. J. Ferguson, T. Kidane, & C. Vye-Brown (Eds.), *Magmatic rifting and active volcanism*, *The Geological Society of London* (Vol. 420, pp. 249–295).
- Castillo, P. R., Klein, E., Bender, J., Langmuir, C., Shirey, S., Batiza, R., & White, W. (2000). Petrology and Sr, Nd, and Pb isotope geochemistry of mid-ocean ridge basalt glasses from the 11°45'N to 15°00'N segment of the East Pacific Rise. *Geochemistry, Geophysics, Geosystems*, *1*(11). <https://doi.org/10.1029/1999GC000024>
- Christie, D. M., & Sinton, J. M. (1981). Evolution of abyssal lavas along propagating segments of the Galapagos Spreading Center. *Earth and Planetary Science Letters*, *56*, 321–335. [https://doi.org/10.1016/0012-821X\(81\)90137-0](https://doi.org/10.1016/0012-821X(81)90137-0)
- Cipriani, A., Brueckner, H., Bonatti, E., & Brunelli, D. (2004). Oceanic crust generated by elusive parents: Sr and Nd isotopes in basalt-peridotite pairs from the Mid-Atlantic Ridge. *Geology*, *32*(8), 657–660. <https://doi.org/10.1130/G20560.1>
- Coogan, L. A., & O'Hara, M. J. (2015). MORB differentiation: In situ crystallization in replenished-tapped magma chambers. *Geochimica et Cosmochimica Acta*, *158*, 147–161. <https://doi.org/10.1016/j.gca.2015.03.010>
- Detrick, R. S., Buhl, P., Vera, E., Mutter, J., Orcutt, J. A., Madsen, J., & Brocher (1987). Multi-channel seismic imaging of a crustal magma chamber along the East Pacific Rise. *Nature*, *326*(6108), 35–41. <https://doi.org/10.1038/326035a0>
- Detrick, R. S., Mutter, J., Buhl, P., & Kim, I. I. (1990). No evidence from multichannel reflection data for a crustal magma chamber in the MARK area on the Mid-Atlantic Ridge. *Nature*, *347*(6288), 61–64. <https://doi.org/10.1038/347061a0>
- Donnelly, K. (2002). The genesis of E-MORB: Extensions and limitations of the hot spot model. (PhD), Columbia, New York.
- Donnelly, K. E., Goldstein, S. L., Langmuir, C. H., & Spiegelman, M. (2004). Origin of enriched ocean ridge basalts and implications for mantle dynamics. *Earth and Planetary Science Letters*, *226*(3–4), 347–366.
- Durant, D. T., & Toomey, D. R. (2009). Evidence and implications of crustal magmatism on the flanks of the East Pacific Rise. *Earth and Planetary Science Letters*, *287*(1–2), 130–136. <https://doi.org/10.1016/j.epsl.2009.08.003>
- Eggs, S. M., Woodhead, J. D., Kinsley, L. P. J., Mortimer, G. E., Sylvester, P., McCulloch, M. T., et al. (1997). A simple method for the precise determination of >40 trace elements in geological samples by ICPMS using enriched isotope internal standards. *Chemical Geology*, *134*(4), 311–326. [https://doi.org/10.1016/S0009-2541\(96\)00100-3](https://doi.org/10.1016/S0009-2541(96)00100-3)
- Ferguson, D. J., Li, Y., Langmuir, C. H., Costa, K. M., McManus, J. F., Huybers, P., & Carbotte, S. M. (2017). A 65 ky time series from sediment-hosted glasses reveals rapid transitions in ocean ridge magmas. *Geology*, *45*(6), 491–494.
- Fornari, D. J., Perfit, M. R., Allan, J. F., & Batiza, R. (1988). Small-scale heterogeneities in depleted mantle sources: near-ridge seamount lava geochemistry and implications for mid-ocean-ridge magmatic processes. *Nature*, *331*(6156), 511–513. <https://doi.org/10.1038/331511a0>

- Gale, A., Dalton, C. A., Langmuir, C. H., Su, Y. J., & Schilling, J.-G. (2013). The mean composition of ocean ridge basalts. *Geochemistry, Geophysics, Geosystems*, 14, 489–518. <https://doi.org/10.1029/2012GC004334>
- Gale, A., Langmuir, C. H., & Dalton, C. A. (2014). The global systematics of ocean ridge basalts and their origin. *Journal of Petrology*, 55(6), 1051–1082. <https://doi.org/10.1093/ptrology/egu017>
- Goss, A. R., Perfit, M. R., Ridley, W. I., Rubin, K. H., Kamenov, G., Soule, S. A., et al. (2010). Geochemistry of lavas from the 2005–2006 eruption at the East Pacific Rise, 9°46'N–9°56'N: Implication for ridge crest plumbing and decadal changes in magma chamber compositions. *Geochemistry, Geophysics, Geosystems*, 11, Q05T09. <https://doi.org/10.1029/2009GC002977>
- Graham, D. W., Zindler, A., Kurz, M. D., Jenkins, W. J., Batiza, R., & Staudigel, H. (1988). He, Pb, Sr and Nd isotope constraints on magma genesis and mantle heterogeneity beneath young Pacific seamounts. *Contributions to Mineralogy and Petrology*, 99(4), 446–463. <https://doi.org/10.1007/BF00371936>
- Hamelin, C., Dosso, L., Hanan, B. B., Barrat, J.-A., & Ondreas, H. (2010). Sr-Nd-Hf isotopes along the Pacific Antarctic Ridge from 41 to 53°N. *Geophysical Research Letters*, 37, L10303. <https://doi.org/10.1029/2010GL042979>
- Han, S., Carbotte, S. M., Carton, H., Mutter, J. C., Aghaei, O., Nedimovic, M. R., & Canales, J. P. (2014). Architecture of on- and off-axis magma bodies at EPR 9°37'–40'N and implications for oceanic crustal accretion. *Earth and Planetary Science Letters*, 390, 31–44. <https://doi.org/10.1016/j.epsl.2013.12.040>
- Hanan, B. B., Blichert-Toft, J., Pyle, D. G., & Christie, D. M. (2004). Contrasting origins of the upper mantle revealed by hafnium and lead isotopes from the Southeast Indian ridge. *Nature*, 432(7013), 91–94. <https://doi.org/10.1038/nature03026>
- Hart, S. R., Blusztajn, J., Dick, H. J. B., Meyer, P. S., & Muehlenbachs, K. (1999). The fingerprint of seawater circulation in a 500-meter section of ocean crust gabbros. *Geochimica et Cosmochimica Acta*, 63(23–24), 4059–4080. [https://doi.org/10.1016/S0016-7037\(99\)00309-9](https://doi.org/10.1016/S0016-7037(99)00309-9)
- Hauri, E. (1996). Major-element variability in the Hawaiian mantle plume. *Nature*, 382(6590), 415–419. <https://doi.org/10.1038/382415a0>
- Hey, R. N., Menard, H. W., Atwater, T. M., & Caress, D. W. (1988). Changes in direction of seafloor spreading revisited. *Journal of Geophysical Research*, 93(B4), 2803–2811. <https://doi.org/10.1029/JB093iB04p02803>
- Hey, R. N., & Wilson, D. S. (1982). Propagating rift explanation for the tectonic evolution of the northeast Pacific—The pseudo-movie. *Earth and Planetary Science Letters*, 58(2), 167–184. [https://doi.org/10.1016/0012-821X\(82\)90192-3](https://doi.org/10.1016/0012-821X(82)90192-3)
- Hirschmann, M. M. (2000). Mantle solidus: Experimental constraints and the effects of peridotite composition. *Geochemistry, Geophysics, Geosystems*, 1(10). <https://doi.org/10.1029/2000GC000070>
- Hirth, G., & Kohlstedt, D. L. (1996). Water in the oceanic upper mantle: Implications for rheology, melt extraction and the evolution of the lithosphere. *Earth and Planetary Science Letters*, 144(1–2), 93–108. [https://doi.org/10.1016/0012-821X\(96\)00154-9](https://doi.org/10.1016/0012-821X(96)00154-9)
- Hofmann, A. W. (1988). Chemical differentiation of the Earth: The relationship between mantle, continental crust, and oceanic crust. *Earth and Planetary Science Letters*, 90(3), 297–314. [https://doi.org/10.1016/0012-821X\(88\)90132-X](https://doi.org/10.1016/0012-821X(88)90132-X)
- Ingle, S., Ito, G., Meahoney, J. J., Chazey, W. J. III, Sinton, J., Rotella, M., & Christie, D. (2010). Mechanisms of geochemical and geophysical variations along the western Galapagos Spreading Center. *Geochemistry, Geophysics, Geosystems*, 11, Q04003. <https://doi.org/10.1029/2009GC002694>
- Jenner, G. A., Fryer, B. J., & McLennan, S. M. (1981). Geochemistry of the Archean Yellowknife Supergroup. *Geochimica et Cosmochimica Acta*, 45(7), 1111–1129. [https://doi.org/10.1016/0016-7037\(81\)90135-6](https://doi.org/10.1016/0016-7037(81)90135-6)
- Katz, R. F., & Weatherley, S. M. (2012). Consequences of mantle heterogeneity for melt extraction at mid-ocean ridges. *Earth and Planetary Science Letters*, 335–336, 226–237. <https://doi.org/10.1016/j.epsl.2012.04.042>
- Klein, E. M., Langmuir, C. H., Zindler, A., Staudigel, H., & Hamelin, B. (1988). Isotopic evidence of a mantle convection boundary at the Australian-Antarctic Discordance. *Nature*, 333(6174), 623–629. <https://doi.org/10.1038/333623a0>
- Langmuir, C. H. (1987). A magma chamber observed. *Nature*, 326(6108), 15–16. <https://doi.org/10.1038/326015a0>
- Langmuir, C. H., Bender, J., Donnelly, K., Shirey, S. B., Cormier, M. H., Baker, E. T., & TEAM, PANR1 (1988). Petrology of the East Pacific Rise north of Orozco transform fault. *Transactions of the American Geophysical Union*, 79, 832.
- Langmuir, C. H., & Bender, J. F. (1984). The geochemistry of oceanic basalts in the vicinity of transform faults: Observations and implications. *Earth and Planetary Science Letters*, 69(1), 107–127. [https://doi.org/10.1016/0012-821X\(84\)90077-3](https://doi.org/10.1016/0012-821X(84)90077-3)
- Langmuir, C. H., Bender, J. F., & Batiza, R. (1986). Petrological and tectonic segmentation of the East Pacific Rise, 5°30'–14°30'N. *Nature*, 322(6078), 422–429. <https://doi.org/10.1038/322422a0>
- Langmuir, C. H., & Hanson, G. N. (1980). An evaluation of major element heterogeneity in the mantle sources of basalts. *Philosophical Transactions. Royal Society of London*, 297(1431), 383–407. <https://doi.org/10.1098/rsta.1980.0223>
- Lissenberg, C. J., MacLeod, C. J., Howard, K. A., & Godard, M. (2013). Pervasive reactive melt migration through fast-spreading lower oceanic crust (Hess Deep, equatorial Pacific Ocean). *Earth and Planetary Science Letters*, 361, 436–447. <https://doi.org/10.1016/j.epsl.2012.11.012>
- Lundstrom, C. C., Sampson, D. E., Perfit, M. R., Gill, J., & Williams, Q. (1999). Insights into mid-ocean ridge basalt petrogenesis: U-series disequilibria from the Siqueiros Transform, Lamont Seamounts, and East Pacific rise. *Journal of Geophysical Research*, 104(B6), 13035–13048. <https://doi.org/10.1029/1999JB900081>
- Macdonald, K. C. (1982). Mid Ocean Ridges: Fine scale tectonic, volcanic and hydrothermal processes within the plate boundary zone. *Annual Reviews in Earth and Planetary Sciences*, 10(1), 155–190. <https://doi.org/10.1146/annurev.ea.10.050182.001103>
- Macdonald, K. C., Fox, P. J., Perram, M. F., Haymon, R. M., Miller, S. P., Carbotte, S. M., et al. (1988). A new view of the mid-ocean ridge from the behavior of ridge-axis discontinuities. *Nature*, 335(6187), 217–225. <https://doi.org/10.1038/335217a0>
- Macdonald, K. C., Scheirer, D. S., & Carbotte, S. M. (1991). Mid-ocean ridges: Discontinuities, segments and giant cracks. *Science*, 253(5023), 986–994. <https://doi.org/10.1126/science.253.5023.986>
- Machado, N., Ludden, J. N., Brooks, C., & Thompson, G. (1982). Fine-scale isotopic heterogeneity in the sub-Atlantic mantle. *Nature*, 295(5846), 226–228. <https://doi.org/10.1038/295226a0>
- Mahoney, J. J., Sinton, J. M., Kurz, M. D., Macdougall, J. D., Spencer, K. J., & Lugmair, G. W. (1994). Isotope and trace element characteristics of a super-fast spreading ridge: East Pacific Rise, 13–23°S. *Earth and Planetary Science Letters*, 121(1–2), 173–193. [https://doi.org/10.1016/0012-821X\(94\)90039-6](https://doi.org/10.1016/0012-821X(94)90039-6)
- McDonough, W. F., & Sun, S.-s. (1995). The composition of the Earth. *Chemical Geology*, 120(3–4), 223–253. [https://doi.org/10.1016/0009-2541\(94\)00140-4](https://doi.org/10.1016/0009-2541(94)00140-4)
- Mégnin, C., & Romanowicz, B. (2000). The 3D shear velocity structure of the mantle from the inversion of body, surface and higher mode waveform. *Geophysical Journal International*, 143(3), 709–728. <https://doi.org/10.1046/j.1365-246X.2000.00298.x>
- Meyzen, C. M., Blichert-Toft, J., Ludden, J. N., Humler, E., Mevel, C., & Albarede, F. (2007). Isotopic portrayal of the Earth's upper mantle flow field. *Nature*, 447(7148), 1069–1074. <https://doi.org/10.1038/nature05920>

- Meysen, C. M., Ludden, J. N., Humler, E., Luais, B., Toplis, M. J., Mevel, C., & Storey, M. (2005). New insights into the origin and distribution of the DUPAL isotope anomaly in the Indian Ocean mantle from MORB of the southwest Indian ridge. *Geochemistry, Geophysics, Geosystems*, 6, Q11K11. <https://doi.org/10.1029/2005GC000979>
- Michael, P. J. (1988). The concentration, behavior and storage of H₂O in suboceanic mantle: Implications for mantle metasomatism. *Geochimica et Cosmochimica Acta*, 52(2), 555–566. [https://doi.org/10.1016/0016-7037\(88\)90110-X](https://doi.org/10.1016/0016-7037(88)90110-X)
- Mougel, B., Agranier, A., Hemond, C., & Gente, P. (2014). A highly unradiogenic lead isotopic signature revealed by volcanic rocks from the East Pacific rise. *Nature Communications*, 5(1), 4474. <https://doi.org/10.1038/ncomms5474>
- Mougel, B., Moreira, M., & Agranier, A. (2015). A “high 4He/3He” mantle material detected under the East Pacific Rise (15°4′N). *Geophysical Research Letters*, 42, 1375–1383. <https://doi.org/10.1002/2014GL062921>
- Niu, Y., & Batiza, R. (1997). Trace element evidence from seamounts for recycled ocean crust in the Eastern Pacific mantle. *Earth and Planetary Science Letters*, 148(3–4), 471–483. [https://doi.org/10.1016/S0012-821X\(97\)00048-4](https://doi.org/10.1016/S0012-821X(97)00048-4)
- Niu, Y., & O'Hara, M. J. (2008). Global correlations of ocean ridge basalt chemistry with axial depth: A new perspective. *Journal of Petrology*, 49(4), 633–664. <https://doi.org/10.1093/ptrology/egm051>
- Niu, Y., Regelous, M., Wendt, I. J., Batiza, R., & O'Hara, M. J. (2002). Geochemistry of near-EPR seamounts: Importance of source vs. process and the origin of enriched mantle component. *Earth and Planetary Science Letters*, 199(3–4), 327–345. [https://doi.org/10.1016/S0012-821X\(02\)00591-5](https://doi.org/10.1016/S0012-821X(02)00591-5)
- O'Hara, M. J. (1977). Geochemical evolution during fractional crystallization of a periodically refilled magma chamber. *Nature*, 266(5602), 503–507. <https://doi.org/10.1038/266503a0>
- O'Neill, H. S. C., & Jenner, F. E. (2012). The global distribution pattern of trace-element distributions in ocean floor basalts. *Nature*, 491(7426), 698–704. <https://doi.org/10.1038/nature11678>
- Payne, J. A., Jackson, M. G., & Hall, P. S. (2013). Parallel volcano trends and geochemical asymmetry of the Society Islands hotspot track. *Geology*, 41(1), 19–22. <https://doi.org/10.1130/G33273.1>
- Perfit, M. R., & Fornari, D. J. (1983). Geochemical studies of abyssal lavas recovered by DSRVALVIN from Eastern Galapagos Rift, Inca Transform, and Ecuador Rift: 2. Phase chemistry and crystallization history. *Journal of Geophysical Research*, 88(B12), 10530–10550. <https://doi.org/10.1029/JB088B12p10530>
- Perfit, M. R., Fornari, D. J., Smith, M. C., Bender, J. F., Langmuir, C. H., & Haymon, R. M. (1994). Small-scale spatial and temporal variations in mid-ocean ridge crest magmatic processes. *Geology*, 22(4), 375–379. [https://doi.org/10.1130/0091-7613\(1994\)022<0375:SSSATV>2.3.CO;2](https://doi.org/10.1130/0091-7613(1994)022<0375:SSSATV>2.3.CO;2)
- Perfit, M. R., Wanless, V. D., Ridley, I. W., Klein, E. M., Smith, M. C., Goss, A. R., et al. (2012). Lava geochemistry as a probe into crustal formation at the East Pacific Rise. *Oceanography*, 25(1), 89–93. <https://doi.org/10.5670/oceanog.2012.06>
- Pertermann, M., Hirschman, M. M., Hametner, K., Günther, D., & Schmidt, M. W. (2004). Experimental determination of trace element partitioning between garnet and silica-rich liquid during anhydrous partial melting of MORB-like eclogite. *Geochemistry, Geophysics, Geosystems*, 5, Q05A01. <https://doi.org/10.1029/2003GC000638>
- Pertermann, M., & Hirschmann, M. M. (2003). Anhydrous partial melting experiments on MORB-like eclogite: Phase relations, phase compositions and mineral-melt partitioning of major elements at 2–3 GPa. *Journal of Petrology*, 44(12), 2173–2201. <https://doi.org/10.1093/ptrology/egg074>
- Pockalny, R. A., Fox, P. J., Fornari, D. J., Macdonald, K. C., & Perfit, M. R. (1997). Tectonic reconstruction of the Clipperton and Siqueiros fracture zones: Evidence and consequences of plate motion change for the last 3 Myr. *Journal of Geophysical Research*, 102(B2), 3167–3181. <https://doi.org/10.1029/96JB03391>
- Regelous, M., Niu, Y., Batiza, R., Greig, A., & Collerson, K. D. (1999). Variations in the geochemistry of magmatism on the East Pacific Rise at 10°30′N since 800 ka. *Earth and Planetary Science Letters*, 168(1–2), 45–63. [https://doi.org/10.1016/S0012-821X\(99\)00048-5](https://doi.org/10.1016/S0012-821X(99)00048-5)
- Reynolds, J., & Langmuir, C. H. (2000). Identification and implications of off-axis lava flows around the East Pacific Rise. *Geochemistry, Geophysics, Geosystems*, 1(6). <https://doi.org/10.1029/1999GC000033>
- Reynolds, J. R. (1995). Segment-scale systematics of mid-ocean ridge magmatism and geochemistry. (PhD), Columbia University.
- Reynolds, J. R., Langmuir, C. H., Bender, J. F., Kastens, K. A., & Ryan, W. B. F. (1992). Spatial and temporal variability in the geochemistry of basalts from the East Pacific Rise. *Nature*, 359(6395), 493–499. <https://doi.org/10.1038/359493a0>
- Rubin, K. H., & Sinton, J. M. (2007). Inferences on mid-ocean ridge thermal and magmatic structure from MORB compositions. *Earth and Planetary Science Letters*, 260(1–2), 257–276. <https://doi.org/10.1016/j.epsl.2007.05.035>
- Rubin, K. H., Sinton, J. M., MacLennan, J., & Hellebrand, E. (2009). Magmatic filtering of mantle compositions at mid-ocean-ridge volcanoes. *Nature Geoscience*, 2(5), 321–328. <https://doi.org/10.1038/ngeo504>
- Rudge, J. F., MacLennan, J., & Stracke, A. (2013). The geochemical consequences of mixing melts from a heterogeneous mantle. *Geochimica et Cosmochimica Acta*, 114, 112–143. <https://doi.org/10.1016/j.gca.2013.03.042>
- Rudge, J. F., McKenzie, D., & Haynes, P. H. (2005). A theoretical approach to understanding the isotopic heterogeneity of mid-ocean ridge basalt. *Geochimica et Cosmochimica Acta*, 69(15), 3873–3887. <https://doi.org/10.1016/j.gca.2005.03.004>
- Saal, A., Hauri, E. H., Langmuir, C. H., & Perfit, M. R. (2002). Vapor undersaturation in primitive mid-ocean ridge basalt and the volatile content of the Earth's upper mantle. *Nature*, 419(6906), 451–455. <https://doi.org/10.1038/nature01073>
- Salters, V. J. M., & Dick, H. J. B. (2002). Mineralogy of the mid-ocean ridge basalt source from neodymium isotopic composition in abyssal peridotites. *Nature*, 418(6893), 68–72. <https://doi.org/10.1038/nature00798>
- Salters, V. J. M., Longhi, J., & Bizimis, M. (2002). Near mantle solidus trace element partitioning at pressures up to 3.4 GPa. *Geochemistry, Geophysics, Geosystems*, 3(7), Q09004. <https://doi.org/10.1029/2001GC000148>
- Salters, V. J. M., & Longhi, J. E. (1999). Trace element partitioning during the initial stages of melting beneath ocean ridges. *Earth and Planetary Science Letters*, 166(1–2), 15–30. [https://doi.org/10.1016/S0012-821X\(98\)00271-4](https://doi.org/10.1016/S0012-821X(98)00271-4)
- Salters, V. J. M., & Stracke, A. (2004). Composition of the depleted mantle. *Geochemistry, Geophysics, Geosystems*, 5, Q05B07. <https://doi.org/10.1029/2003GC000597>
- Schilling, J.-G. (1975). Azores mantle blob: The rare earth evidence. *Earth and Planetary Science Letters*, 25(2), 103–115. [https://doi.org/10.1016/0012-821X\(75\)90186-7](https://doi.org/10.1016/0012-821X(75)90186-7)
- Schilling, J.-G., Fontignie, D., Blichert-Toft, J., Kingsley, R., & Tomza, U. (2003). Pb-Hf-Nd-Sr isotope variations along the Galápagos Spreading Center (101°–83°W): Constraints on the dispersal of the Galápagos mantle plume. *Geochemistry, Geophysics, Geosystems*, 4(10), 8512. <https://doi.org/10.1029/2002GC000495>
- Schilling, J.-G., Kingsley, R., Fontignie, D., Poreda, R., & Xue, S. (1999). Dispersion of the Jan Mayen and Iceland mantle plumes in the Arctic: A He=Pb-Nd-Sr isotope tracer study of basalts from the Kolbeinsey, Mohns, and Knipovich Ridges. *Journal of Geophysical Research*, 104(B5), 10543–10569. <https://doi.org/10.1029/1999JB900057>

- Schilling, J.-G., Zajac, M., Evans, R., Johnston, T., White, W., Devine, J. D., & Kingsley, R. (1983). Petrological and geochemical variations along the Mid-Atlantic ridge from 29°N to 73°N. *American Journal of Science*, 283(6), 510–586. <https://doi.org/10.2475/ajs.283.6.510>
- Schouten, H., & Klitgord, K. D. (1982). The memory of the accreting plate boundary and the continuity of fracture-zones. *Earth and Planetary Science Letters*, 59(2), 255–266. [https://doi.org/10.1016/0012-821X\(82\)90130-3](https://doi.org/10.1016/0012-821X(82)90130-3)
- Shimizu, K., Saal, A. E., Myers, C. E., Nagle, A. N., Hauri, E. H., Forsyth, D. W., et al. (2016). Two-component mantle melting-mixing model for the generation of mid-ocean ridge basalts: Implications for the volatile content of the Pacific upper mantle. *Geochimica et Cosmochimica Acta*, 176, 44–80. <https://doi.org/10.1016/j.gca.2015.10.033>
- Shorttle, O., & MacLennan, J. (2011). Compositional trends of Icelandic basalts: Implications for short length scale lithological heterogeneity in mantle plumes. *Geochemistry, Geophysics, Geosystems*, 12, Q11008. <https://doi.org/10.1029/2011GC003748>
- Shorttle, O., MacLennan, J., & Piotrowski, A. M. (2013). Geochemical provincialism in the Iceland plume. *Geochimica et Cosmochimica Acta*, 122, 363–397. <https://doi.org/10.1016/j.gca.2013.08.032>
- Sims, K. W. W., Blichert-Toft, J., Fornari, D. J., Perfit, M. R., Goldstein, S. J., Johnson, P., et al. (2003). Aberrant youth: Chemical and isotopic constraints on the origin of off-axis lavas from the East Pacific Rise, 9°–10°N. *Geochemistry, Geophysics, Geosystems*, 4(10), 8621. <https://doi.org/10.1029/2002GC000443>
- Sims, K. W. W., Goldstein, S. J., Blichert-Toft, J., Perfit, M. R., Kelemen, P. B., Fornari, D., et al. (2002). Chemical and isotopic constraints on the generation and transport of magma beneath the East Pacific rise. *Geochimica et Cosmochimica Acta*, 66(19), 3481–3504. [https://doi.org/10.1016/S0016-7037\(02\)00909-2](https://doi.org/10.1016/S0016-7037(02)00909-2)
- Singh, S. C., Crawford, W. C., Carton, H., Seher, T., Combier, V., Cannat, M., et al. (2006). Discovery of a magma chamber and faults beneath a Mid-Atlantic ridge hydrothermal field. *Nature*, 442(7106), 1029–1032. <https://doi.org/10.1038/nature05105>
- Sinton, J., Bergmanis, E. C., Rubin, K. H., Batiza, R., Gregg, T. K. P., Gronvold, K., et al. (2002). Volcanic eruptions on mid-ocean ridges: New evidence from the superfast spreading East Pacific Rise, 17°–19°S. *Journal of Geophysical Research*, 107(B6), 2115. <https://doi.org/10.1029/2000JB000090>
- Sinton, J., Detrick, R., Canales, J. P., Ito, G., & Behn, M. (2003). Morphology and segmentation of the western Galapagos Spreading Center, 90.5°–98°W: Plume-ridge interaction at an intermediate spreading ridge. *Geochemistry, Geophysics, Geosystems*, 4(12), Q04003. <https://doi.org/10.1029/2003GC000609>
- Sinton, J. M., & Detrick, R. S. (1992). Mid-ocean ridge magma chambers. *Journal of Geophysical Research*, 97(B1), 197–216. <https://doi.org/10.1029/91JB02508>
- Sinton, J. M., Smaglik, S. M., Mahoney, J. J., & Macdonald, K. C. (1991). Magmatic processes at superfast spreading mid-ocean ridges: Glass compositional variations along the East Pacific Rise 13°–23°S. *Journal of Geophysical Research*, 96(B4), 6133–6155. <https://doi.org/10.1029/90JB02454>
- Smith, M. C., Perfit, M. R., Fornari, D. J., Ridley, W. I., Edwards, M. H., Kurras, G. J., & Von Damm, K. L. (2001). Magmatic processes and segmentation at a fast spreading mid-ocean ridge: Detailed investigation of an axial discontinuity on the East Pacific Rise crest at 9°37'N. *Geochemistry, Geophysics, Geosystems*, 2(10). <https://doi.org/10.1029/2000GC000134>
- Smith, S. E., Casey, J. R., Bryan, W. B., Dmitriev, L., Silant'ev, S., & Magakyan, R. (1998). Geochemistry of basalts from the Hayes transform region of the Mid-Atlantic Ridge. *Journal of Geophysical Research*, 103(B3), 5305–5329. <https://doi.org/10.1029/97JB03208>
- Spiegelman, M., & Kelemen, P. B. (2003). Extreme chemical variability as a consequence of channelized melt transport. *Geochemistry, Geophysics, Geosystems*, 4(7), 1055. <https://doi.org/10.1029/2002GC000336>
- Stracke, A., Bizimis, M., & Salters, V. J. M. (2003). Recycling oceanic crust: Quantitative constraints. *Geochemistry, Geophysics, Geosystems*, 4(3), 8003. <https://doi.org/10.1029/2001GC000223>
- Stracke, A., & Bourdon, B. (2009). The importance of melt extraction for tracing mantle heterogeneity. *Geochimica et Cosmochimica Acta*, 73(1), 218–238. <https://doi.org/10.1016/j.gca.2008.10.015>
- Stracke, A., Snow, J. E., Hellebrand, E., von der Handt, A., Bourdon, B., Birbaum, K., & Günther, D. (2011). Abyssal peridotite Hf isotopes identify extreme mantle depletion. *Earth and Planetary Science Letters*, 308(3–4), 359–368. <https://doi.org/10.1016/j.epsl.2011.06.012>
- Stracke, A., Zindler, A., Salters, V. J. M., McKenzie, D., Blichert-Toft, J., Albarède, F., & Grönvold, K. (2003). Theistareykir revisited. *Geochemistry, Geophysics, Geosystems*, 4(2), 8507. <https://doi.org/10.1029/2001GC000201>
- Sturm, M. E., Klein, E. M., Graham, D. W., & Karsten, J. (1999). Age constraints on crustal recycling to the mantle beneath the southern Chile Ridge: He-Pb-Sr-Nd isotope systematics. *Journal of Geophysical Research*, 104(B3), 5097–5114. <https://doi.org/10.1029/1998JB900107>
- Su, Y. J. (2002). *Mid-ocean ridge basalt trace element systematics: Constrain from database management, ICPMS analyses, global data compilation and petrologic modeling*. (PhD). New York: Columbia University.
- Todt, W., Cliff, R. A., Hanserr, A., & Hofmann, A. W. (1996). Evaluation of a 202Pb–205Pb double spike for high-precision lead isotope analysis. In S. Hart & A. Basu (Eds.), *Earth processes, reading the isotope record* (Vol. 95, pp. 429–437). Washington, DC: American Geophysical Union.
- Toomey, D. R., Jousset, D., Dunn, R. A., Wilcock, W. S. D., & Detrick, R. S. (2007). Skew of mantle upwelling beneath the East Pacific Rise governs segmentation. *Nature*, 446(7134), 409–414. <https://doi.org/10.1038/nature05679>
- Turner, S., Beier, C., Niu, Y., & Cook, C. (2011). U-Th-Ra disequilibrium and the extent of off-axis volcanism across the East Pacific Rise at 9°30'N, 10°30'N, and 11°20'N. *Geochemistry, Geophysics, Geosystems*, 12, Q0AC12. <https://doi.org/10.1029/2010GC003403>
- Wanless, V. D., Perfit, M. R., Klein, E. M., White, S., & Ridley, I. W. (2012). Reconciling geochemical and geophysical observations of magma supply and melt distribution at the 9°N overlapping spreading center, East Pacific Rise. *Geochemistry, Geophysics, Geosystems*, 13, Q11005. <https://doi.org/10.1029/2012GC004168>
- Wanless, V. D., Perfit, M. R., Ridley, I. W., & Klein, E. M. (2010). Dacite petrogenesis on mid-ocean ridges: Evidence for oceanic crustal melting and assimilation. *Journal of Petrology*, 51(12), 2377–2410. <https://doi.org/10.1093/petrology/egq056>
- Wanless, V. D., & Shaw, A. M. (2012). Lower crustal crystallization and melt evolution at mid-ocean ridges. *Nature Geoscience*, 5(9), 651–655. <https://doi.org/10.1038/ngeo1552>
- Waters, C. L., Sims, K. W. W., Perfit, M. R., Blichert-Toft, J., & Blusztajn, J. (2011). Perspective on the genesis of E-MORB from chemical and isotopic heterogeneity at 9–10°N East Pacific Rise. *Journal of Petrology*, 52(3), 565–602. <https://doi.org/10.1093/petrology/egq091>
- Waters, C. L., Sims, K. W. W., Soule, S. A., Blichert-Toft, J., Dunbar, N., Plank, T., et al. (2013). Recent volcanic accretion at 9–10°N East Pacific Rise as resolved by combined geochemical and geological observations. *Geochemistry, Geophysics, Geosystems*, 14, 2547–2574. <https://doi.org/10.1002/ggge.20134>

- Weis, D., Garcia, M. O., Rhodes, J. M., Jellinek, M., & Scoates, J. S. (2011). Role of the deep mantle in generating the compositional asymmetry of the Hawaiian mantle plume. *Nature Geoscience*, 4(12), 831–838. <https://doi.org/10.1038/ngeo1328>
- Wendt, J. I., Regelous, M., Niu, Y., Hékinian, R., & Collerson, K. D. (1999). Geochemistry of lavas from the Garrett transform fault: Insights into mantle heterogeneity beneath the eastern Pacific. *Earth and Planetary Science Letters*, 173(3), 271–284. [https://doi.org/10.1016/S0012-821X\(99\)00236-8](https://doi.org/10.1016/S0012-821X(99)00236-8)
- White, S. M., Haymon, R. M., Fornari, D. J., Perfit, M. R., & Macdonald, K. C. (2002). Correlation between volcanic and tectonic segmentation of fast-spreading ridges: Evidence from volcanic structures and lava flow morphology of the East Pacific rise at 9°–10°N. *Journal of Geophysical Research*, 107(B8), 2173. <https://doi.org/10.1029/2001JB000571>
- Zhang, Y., Meng, F., & Niu, Y. (2016). Hf isotope systematics of seamounts near the East Pacific Rise (EPR) and geodynamic implications. *Lithos*, 262, 107–119. <https://doi.org/10.1016/j.lithos.2016.06.026>
- Zimmer, M., Kröner, A., Jochum, K. P., Reischmann, T., & Todt, W. (1995). The Gabal-Gerf Complex—A Precambrian N-MORB ophiolite in the Nubian Shield, NE Africa. *Chemical Geology*, 123(1–4), 29–51. [https://doi.org/10.1016/0009-2541\(95\)00018-H](https://doi.org/10.1016/0009-2541(95)00018-H)
- Zindler, A., Staudigel, H., & Batizza, R. (1984). Isotope and trace element geochemistry of young Pacific seamounts: Implications for the scale of upper mantle heterogeneity. *Earth and Planetary Science Letters*, 70(2), 175–195. [https://doi.org/10.1016/0012-821X\(84\)90004-9](https://doi.org/10.1016/0012-821X(84)90004-9)
- Zou, H., Zindler, A., & Niu, Y. (2002). Constraints on melt movement beneath the East Pacific Rise from ^{230}Th - ^{238}U disequilibrium. *Science*, 295(5552), 107–110. <https://doi.org/10.1126/science.1064295>